Soft Matter

PAPER

View Article Online
View Journal

Cite this: DOI: 10.1039/d4sm00837e

Light scattering study of algal floc growth and structure: alum *vs.* polymeric plant-derived flocculant†

Temitope Orimolade,[a] Ngoc-Tram Le,[a] Lyle Trimble,[a] Bandaru Ramarao[b] and Sitaraman Krishnan *[a]

Received 10th July 2024,
Accepted 24th October 2024

DOI: 10.1039/d4sm00837e

rsc.li/soft-matter-journal

The flocculation dynamics of *Microcystis aeruginosa* algal cultures using alum and aqueous *Moringa oleifera* seed extracts as flocculants were analyzed through light scattering and fractal analysis. Floc growth in continuously stirred *M. aeruginosa* suspensions, with cell densities ranging from 200 to 800 μg L^{-1} chlorophyll *a* (Chl *a*), exhibited distinct patterns in fractal dimension (d_F) evolution relative to floc size: a smooth, monotonic increase; stochastic increase; and stabilization or leveling off. d_F values ranged from 1.3 to 2.6, with floc diameters ($D_{4,3}$ volume-weighted mean) spanning 30 to 300 μm. Alum (0.1 to 0.4 g L^{-1}) induced fast diffusion-limited flocculation, initially producing lower d_F values, which progressively increased due to structural rearrangement at a slower rate. In contrast, at sufficiently high concentrations (0.1 to 0.2 g L^{-1} BSA equivalent), *M. oleifera* seed proteins facilitated stable, high $d_F \approx 2.0$ early on, evidently through patch charge interactions. Flocs formed with alum were prone to shear-induced breakage, limiting both their size and stability, whereas *M. oleifera* extract produced larger, more stable flocs with greater resilience to shear due to robust particle network formation by the polymer. Both flocculants effectively treated 800 μg L^{-1} Chl *a* *M. aeruginosa* suspensions, but *M. oleifera* extract demonstrated better performance in terms of floc size at similar mass concentrations. These findings highlight the potential of *Moringa* seed extract as a sustainable and effective alternative to conventional flocculants like alum, offering insights into their mechanisms and performance in flocculation processes.

1 Introduction

1.1 Algal cell flocculation in environmental remediation

Harmful algal blooms (HABs) represent a critical environmental challenge, characterized by the rapid proliferation of algae in aquatic ecosystems, leading to adverse impacts on water quality and ecosystem health.[1] Among the common algal species contributing to HABs is *Microcystis aeruginosa*, a cyanobacterium known for its ability to produce toxins, particularly microcystins, which pose significant risks to human health and the environment. Traditional approaches to mitigate algal blooms, such as the use of chlorine-based disinfectants, can inadvertently release endotoxins from cell lysis, produce cell debris that can foul and clog membranes used in downstream purification processes, and also result in toxic disinfection byproducts in the treated water.[2]

In this context, exploring natural alternatives to chemical treatments has garnered significant interest. One promising candidate is the seed of *Moringa oleifera*, known for its coagulation and flocculation properties. The seeds contain relatively low molecular weight (6.5 to 29 kg mol^{-1}) proteins[3] such as MO2 and Mo-CBP3 that are rich in arginine and glutamine (Table S1, ESI†) and, therefore, exhibit cationic properties, and can effectively aid in the flocculation of algae cells.[4–6] Flocculation using organic flocculant not only remediates aquatic environments by removing the algal cells but also facilitates their harvest for valorization as biorefinery feedstock.[7,8]

1.2 Comparative analysis of inorganic and organic flocculants

Inorganic flocculants like aluminum sulfate and polyaluminum chloride have been used for flocculating algae[9,10] and can be used for treating HAB-infested water. Aluminum chloride

[a] Clarkson University, Department of Chemical & Biomolecular Engineering, 8 Clarkson Avenue, Potsdam, NY 13699, USA. E-mail: skrishna@clarkson.edu; Tel: +1 315 268 6661

[b] SUNY College of Environmental Science & Forestry, Department of Chemical Engineering, 1 Forestry Drive, Syracuse, NY 13210, USA

† Electronic supplementary information (ESI) available: Includes details on *M. oleifera* seed proteins, seed extract properties, size distribution in *M. aeruginosa* suspensions at different cell concentrations, jar test results, and profiles of volume distribution, diameter, and fractal dimension evolution. See DOI: https://doi.org/10.1039/d4sm00837e

effectively treats *M. aeruginosa* without causing cell lysis or toxin release if flocs are removed immediately, though toxin release occurs after a few days of contact.[10] However, aluminum salts have high carbon footprints, operating costs,[11] and could pose health risks in drinking water.[12] Additionally, improper disposal of alum sludge leads to environmental pollution. In contrast, organic polyelectrolytes and natural polymeric flocculants produce less sludge.[4] Natural polymeric flocculants, in particular, are biodegradable, non-toxic, and offer both cost and environmental benefits.[8,13,14] Furthermore, they generally do not significantly alter the pH and conductivity of treated water.

1.3 Research gap and study objective

Some prior studies have addressed the flocculation of *M. aeruginosa* using *Moringa*,[15,16] but there remains a need for more detailed investigations into the impact of flocculant dosing on flocculation kinetics, floc size, and structure, including a cross-comparison with alum. Inorganic flocculants like alum primarily work through charge neutralization, reducing surface charges and allowing particles to aggregate by minimizing electrostatic repulsion. High molecular weight polymeric flocculants often mediate bridging flocculation, where a polymer chain adsorbs onto surfaces of different particles, linking them together. Cationic polymers, such as *M. oleifera* proteins, bind to anionic cell surfaces, creating areas of positive and negative charges. Patch charge flocculation occurs when patches of opposite charges on different particles attract each other, leading to aggregation.[17] These differing mechanisms affect the kinetics of aggregate growth, as well as the floc structure and strength. To our knowledge, no prior reports compare these aspects of *M. aeruginosa* flocculation using alum *versus Moringa* seed proteins, or detail the evolution of the floc structure of the algal cells in the presence of these flocculants. The trends in the evolution of the fractal dimensions of *M. aeruginosa* flocs during flocculation are also unknown. This study examined the flocculation dynamics of *M. aeruginosa* with *M. oleifera* seed extract at various protein and algal cell concentrations. The results were compared to those from similar experiments using alum.

1.4 Flocculation dynamics

Chakraborti *et al.*[18] studied the temporal changes in fractal dimension during the flocculation of polystyrene latex microparticles (approximately 10 μm in diameter) using alum as a flocculant. They employed optical sampling and digital image analysis to observe two-dimensional fractal dimension variations under different mixing speeds, coagulant doses, and particle concentrations. For the aggregation of an initially monodisperse suspension, they found the expected increase in floc size with alum dose. However, the fractal dimension decreased over 30 min of flocculation.

Selomulya *et al.*[19] developed a mathematical model using population balance equations to analyze the flocculation dynamics of submicron polymer latex particles induced by $MgCl_2$. An increase in d_F throughout 40 min of flocculation was observed. They investigated two key mechanisms affecting floc characteristics: (1) restructuring, where particles or clusters rotate about their contact points without disintegrating, facilitating the formation of additional bonds with neighboring particles; and (2) break-up followed by re-aggregation into a more compact structure. Their findings suggested that restructuring primarily influenced floc densitification in the initial stages when floc sizes were small. In contrast, floc break-up and subsequent re-aggregation played a more significant role in structural densification under conditions involving larger particles and higher shear rates.

Lattuada *et al.*[20] investigated NaCl-induced flocculation of polystyrene and fluoropolymer latexes with primary particle sizes ranging from 70 to 250 nm, using light scattering measurements. They analyzed the time-dependent evolution of the scattering structure factor (instead of fractal dimension) to investigate changes in floc size and structure over time. Their findings indicated that the measured evolution of the structure factor, obtained through static light scattering measurements, closely matched simulation results where aggregation was modeled as a second-order kinetics process. The model distinguished between scenarios with no repulsive interactions among particles (fast diffusion-limited cluster aggregation) and those with repulsive interactions (reaction-limited cluster aggregation).

Antunes *et al.*[21,22] utilized light scattering to examine the flocculation of calcium carbonate particles with high-molecular-weight polyelectrolytes, investigating the impact of flocculant dosage, polymer branching, and medium cationic content on floc structure. Like Selomulya *et al.*,[19] their studies highlighted the use of the fractal dimension or scattering exponent as an indicator of aggregate structure and behavior during flocculation.

Metaxas *et al.*[23] explored the flocculation of sodium bentonite particles using high-molecular-weight cationic polyacrylamide in Taylor–Couette cells under laminar and turbulent flow conditions. Through laser light sheet imaging and analysis, they observed nearly time-invariant behavior in the surface-based fractal dimension across different flow Reynolds numbers during the flocculation process.

1.5 Analytical framework for the current study

The literature reviewed highlights various methodologies and insights into fractal dynamics during flocculation processes. Given the effectiveness of static light scattering for rapid sampling and real-time measurement of floc size distribution and three-dimensional fractal dimension in flocculating systems, we adopted this method for studying algal cell aggregates.

In characterizing floc structure using light scattering, individual fractal aggregates comprising k primary particles of radius a exhibit a power law decay of scattering intensity with the magnitude, q, of the scattering wave vector according to

$$I_k(q) = \frac{k^2 I_1}{(qa_k)^{d_F}} = \frac{kI_1}{(qa)^{d_F}} \quad (1)$$

where I_k is the scattering intensity of the aggregate, I_1 is the scattering intensity of a single spherical primary particle, a_k is the size of the aggregate of k primary particles, and d_F is the fractal dimension of the aggregate.[24] The fractal behavior is

observed in the q range of

$$\frac{1}{a} > q > \frac{1}{a_k} \tag{2}$$

where q is related to the scattering angle, θ, the *in vacuo* light wavelength, λ_0, and the refractive index of the medium, n, by

$$q = \frac{4\pi n}{\lambda_0} \sin\left(\frac{\theta}{2}\right) \tag{3}$$

In the fractal regime,

$$\frac{a_k}{a} = k^{1/d_F} \tag{4}$$

The fractal dimension is generally lower than the Euclidean dimensionality and depends on the aggregation mechanism and floc structure. Simulations and experiments have shown that flocs formed by diffusion-limited cluster–cluster aggregation typically have $d_F \approx 1.75$, while those formed by reaction-limited aggregation are more compact with $d_F \approx 2.1$.[25–27] In reaction-limited aggregation, interacting moieties sample many configurations before flocculating, resulting in denser aggregates. Additionally, weak interparticle interactions allowing internal restructuring can increase d_F.

The total scattering intensity is given by

$$I(q) = \sum n_k I_k(q) = \frac{I_0}{(qa)^{d_F}} \tag{5}$$

where $I_0 = n_0 I_1$ and $n_0 = \sum (k n_k)$. Therefore, $I(q)$ would be independent of the aggregate size and display a linear relationship with a slope of $-d_F$ on a log–log plot of $I(q)$ *vs.* q. Given the possibility that the aggregate structure is no longer fractal when breakage and restructuring occur, the value of the experimental linear slope has been referred to as the scattering exponent rather than the fractal dimension.[22] Nevertheless, for the sake of conceptual familiarity and consistency, the term "fractal dimension" will be maintained while acknowledging this distinction.

In this study, scattered intensity data were analyzed to track the time evolution of floc size and fractal dimension, enabling a detailed comparison of the two types of flocculants. The floc compactness, indicated by fractal dimension, varies with floc size, aggregation and fragmentation rates, shear forces, and particle bonding.[19] Specifically, this research investigated differences in bonding mechanisms induced by alum and the *Moringa oleifera* protein under identical flow conditions.

2 Results and discussion

2.1 Extraction and properties of *M. oleifera* seed flocculant

M. oleifera seeds contain up to 40 wt% lipids, including different fatty acids,[28] that are not flocculative but would increase the organic matter in treated water. These lipids were separated from the seeds in a deoiling step that involved extraction of the lipids in ethanol (see Section 4 for materials and methods). Water extraction of the deoiled seeds yielded the deoiled *M. oleifera* seed extract (DMSE) for flocculation studies (Fig. S1, ESI†). The protein concentration in DMSE, measured in BSA equivalents, was 16 ± 2 g L^{-1} (Fig. S2, ESI†).

Organic flocculants can reduce the surface tension of a dispersion, potentially influencing the flocculation mechanism through interfacial adsorption and the formation of air bubbles. The surface tension of the undiluted extract in 1 M aqueous NaCl solution was approximately 57.5 mN m^{-1}, increasing as the protein concentration decreased, as illustrated in Fig. S3 (ESI†). The results indicate that within the concentration range of 0.032–0.128 g L^{-1} employed in the flocculation studies (*vide infra*), the reduction in surface tension would be minimal. Thus, DMSE would predominantly adsorb at the cell–water interface rather than the air–water interface, thereby promoting flocculation without the concerns of air bubble formation, which could otherwise impact flocculation dynamics, floc structure, and complicate light scattering analysis.

2.2 Particle size distribution in flocculant-free *M. aeruginosa* suspensions

The size distributions of cells in *M. aeruginosa* suspensions were determined using light scattering, with a particle refractive index of 1.56 and absorptivity of 0.000133.[29] The 200 μg L^{-1} Chl *a* suspension contained unaggregated cells, with the primary particle diameter centered around 4 μm, consistent with optical microscopy observations. The average cell diameter, determined from optical microscopy images (Fig. 1(a)) using the ImageJ software,[30] was 4.5 ± 0.8 μm. In suspensions with higher cell densities (400 and 800 μg L^{-1} Chl *a*), a secondary population of larger flocs, stable against disintegration at 70 rpm stirring speed was observed even without adding any flocculant (Fig. 2).

Table 1 gives the particle diameters and obscuration for the *M. aeruginosa* suspensions at three different concentrations. All values exhibited temporal variations (see Fig. S4 and S5, ESI†).

We used obscuration data to estimate the cell density in *M. aeruginosa* suspension. For 4 μm diameter particles of complex relative refractive index $m = 1.17 + 0.0001i$,[29] $Q_{sca} \approx 1.994$ and $Q_{abs} \approx 0.009$ (Fig. S6, ESI†), resulting in $Q_{ext} \approx 2.003$. The path length, b, was approximately 2.4 mm, determined by measuring the obscuration of monodisperse polystyrene latex standard of known particle size and concentration. Using these values, the cell number concentration in the 200 μg L^{-1} Chl *a* suspension was estimated to be 8.5×10^5 cells per mL. Assuming an order of dependence of 0.53 on Chl *a* concentration,[31] the number density for 800 μg L^{-1} Chl *a* would be $\approx 1.8 \times 10^6$ cells per mL. These densities fall within the range identified by the New York State Department of Environmental Conservation and the World Health Organization as having a high probability of adverse health effects (50–5000 μg L^{-1} Chl *a*, 10^5–10^7 cells per mL).[32] Estimated cell volume fractions ranged from 0.0028% to 0.006%.

2.3 Flocculant concentration range selection, floc volume distribution, and fractal dimension determination

Flocculant concentrations were screened using jar tests and optical microscopy (Section S5, ESI†). Alum concentrations from 0.1 to 0.4 g L^{-1}, based on the volume of *M. aeruginosa* cell suspension treated, were found suitable for the target cell densities.

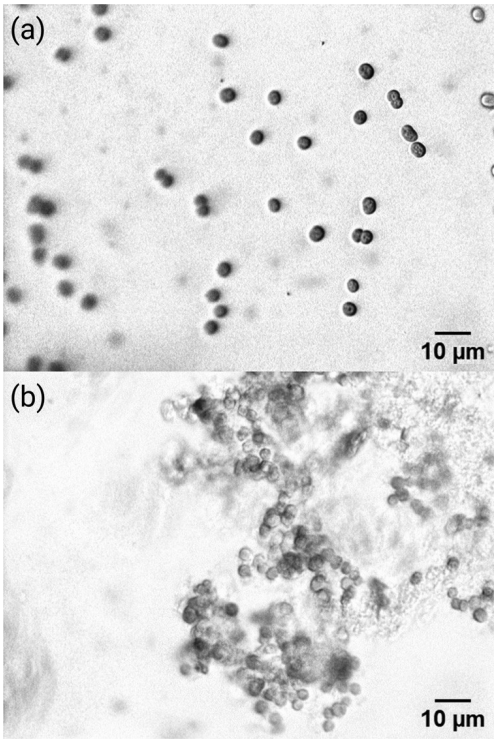

Fig. 1 Optical microscopy images of *M. aeruginosa* cell suspensions at 800 μg L^{-1} Chl *a*: (a) without and (b) with 2 mL L^{-1} DMSE.

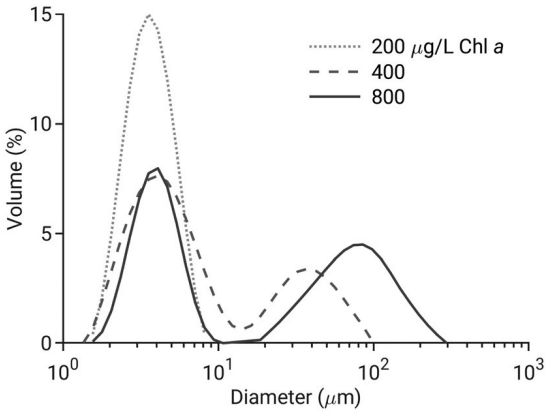

Fig. 2 Steady-state size distributions of cells and flocs in *M. aeruginosa* cell suspensions with cell concentrations of 200, 400, and 800 μg L^{-1} Chl *a*, in the absence of added flocculant; 70 rpm, 3035 s.

Although higher than typical water treatment concentrations (0.01–0.05 g L^{-1}), this interval has been effective for microalgae harvesting by flocculation and sedimentation.[33] DMSE dosages ranged from 2 to 8 mL L^{-1}. Given a protein concentration of approximately 16 g L^{-1} in the extract, these dosages correspond to the protein mass concentrations of 0.032 to 0.128 g L^{-1}.

Jar tests demonstrated complete settling within 1 h for flocs formed from 800 μg L^{-1} Chl *a M. aeruginosa* suspensions with 0.1 g L^{-1} alum or 2 mL L^{-1} DMSE. The floc diameters ($D_{4,3}$) in these cases were about 218 μm with alum and 83 μm with DMSE, indicating that these sizes are sufficiently large for floc

Table 1 Particle diameters and obscuration in *M. aeruginosa* cultures with different cell densities (no added flocculant)[a]

Chl *a* (μg L^{-1})	200	400	800
$D_{4,3}$ (μm)	3.83(3)	15.1(5)	43(1)
$D_{3,2}$ (μm)	3.41(3)	5.1(1)	6.7(1)
$d_{0.5}$ (μm)	3.60(4)	5.4(2)	6.9(4)
$d_{0.9}$ (μm)	5.68(9)	45(1)	118(5)
Obscuration (%)	4(1)	9.1(1)	15.4(1)

[a] Averages from data collected during 2000–3000 s of stirring at 70 rpm. Numbers in parentheses indicate uncertainty in the last significant digit. Refer to the Methods section (Section 4.2) for definitions of the variables presented in this table.

removal within 1 h of settling. Optical microscopy observations indicated the presence of isolated spherical cells or pairs in the absence of a flocculant, while cell aggregates formed upon adding the flocculant (Fig. 1). This change in structure was further supported by obscuration data from light scattering experiments, which also indicated the occurrence of flocculation. Fig. 3 shows obscuration *vs.* time profiles for the 800 μg L^{-1} Chl *a* suspension using different concentrations of alum and DMSE. With alum, obscuration generally decreased over time, but DMSE showed non-monotonic trends, especially at concentrations of 6 and 8 mL L^{-1}.

The obscuration data were collected under the same experimental conditions as the other light scattering experiments in this study (Section 4.2) as opposed to the quiescent settling typically associated with conventional sedimentation. These flow conditions allow for dynamic floc formation and breakage during measurements, which may account for the observed non-monotonic trends.

In general, obscuration decreases with a reduction in the number of primary particles (individual *M. aeruginosa* cells) by flocculation but increases as the size of flocs formed during flocculation grows. The increase in obscuration due to a higher flocculant dosage is clearly evident in the later time data for DMSE, presented in Fig. 3(b). However, the trends observed with alum [Fig. 3(a)] are more complex, reflecting the combined effects of number density, floc size, and floc size distribution. This highlights the need for a more detailed analysis of the light scattering data, specifically in terms of floc size distributions, to gain a deeper understanding of the flocculation mechanisms involved.

Floc size distributions were determined using Mie-theory-based size deconvolution of scattered light intensity *versus* angle data, collected approximately every 74 s throughout the flocculation process. In most experiments, data were collected for up to about 4366 s, corresponding to 59 intervals after the initial measurement, for a total of 60 measurements. Fig. 4 shows the time evolution of volume distributions for *M. aeruginosa* suspensions with alum and DMSE. The shift toward larger particle diameters is evident, with the primary particle peak decreasing and the floc peak shifting right and increasing. All floc size distribution evolutions for alum and DMSE discussed in this article are detailed in Fig. S8 and S11 (ESI†), respectively.

Fractal dimensions were determined from the time evolution of the scattered intensity at various scattering angles. In

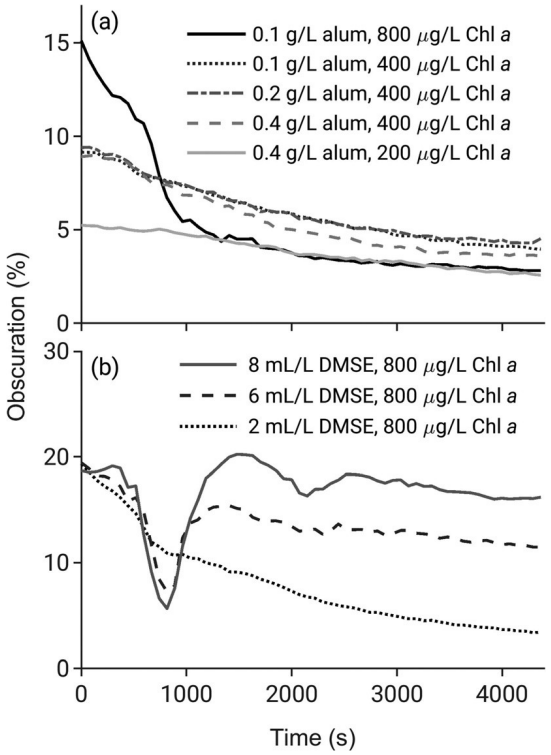

Fig. 3 Time evolution of obscuration in *M. aeruginosa* suspensions flocculated using (a) alum and (b) DMSE at various cell densities and flocculant concentrations.

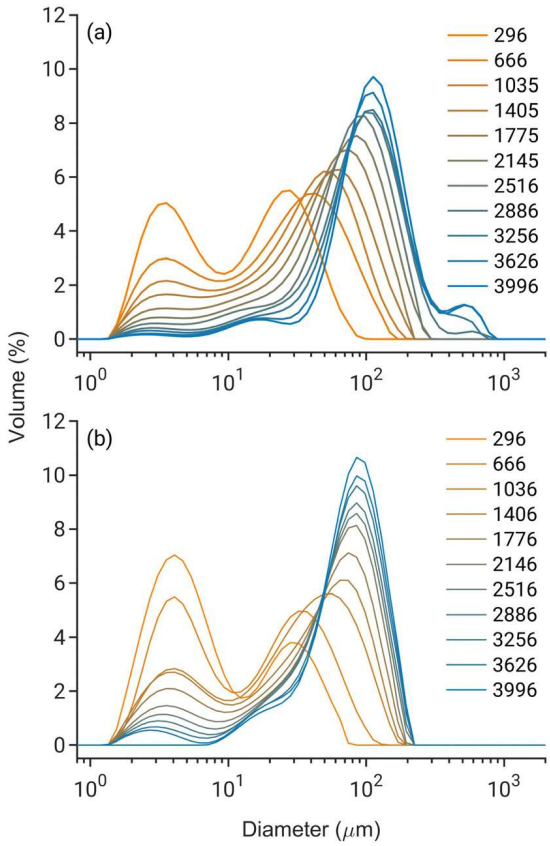

Fig. 4 Evolution of floc size distribution during flocculation of *M. aeruginosa* with (a) 200 μg L^{-1} Chl *a* cell density and 0.4 g L^{-1} alum, and (b) 800 μg L^{-1} Chl *a* cell density and 2 mL L^{-1} DMSE. The numbers in the legend indicate time (in seconds) elapsed during the flocculation process.

Fig. 5, the evolution of $I(q)$ *vs.* q for *M. aeruginosa* flocs using alum is shown. The q range to determine the scattering exponent was chosen based on a coefficient of determination $R^2 > 0.99$ from a linear regression of $\log[I(q)]$ on $\log(q)$. The upper limit for the fractal range would be the inverse of the radius of the primary particles, ≈ 0.5 μm^{-1}, given a particle diameter of 4 μm for the *M. aeruginosa* cells. The range of 0.1 to 0.5 μm^{-1} was found to exhibit a linear behavior for most datasets, particularly after about 500 s when the flocs had grown sufficiently. For larger floc sizes, the q range shifted slightly towards lower values to include data with higher scattering intensities.

2.4 Evolution of floc size using alum flocculant

Diameters $D_{4,3}$, $D_{3,2}$, $d_{0.5}$, and $d_{0.9}$ of the flocs were calculated from volume distributions corresponding to different flocculation time, t. Changes in $D_{4,3}$ and $d_{0.5}$ during flocculation exhibited comparable trends, bounded by the $d_{0.9}$ and $D_{3,2}$ profiles (see Fig. S9, ESI†). $D_{4,3}$ was selected as the measure of floc size, and its time evolution was analyzed. Fig. 6(a)–(c) shows that for alum, floc sizes gradually increased over time when *M. aeruginosa* density was 200 or 400 μg L^{-1} Chl *a*. However, at the highest cell density (800 μg L^{-1} Chl *a*), there was an abrupt jump from about 121 μm [point 1 in Fig. 6(a)] to 214 μm (point 2) with 0.1 g L^{-1} alum.

This abrupt increase in floc size, as evidenced by the $D_{4,3}$ profile, suggests rapid coalescence at a specific point in time, likely associated with the particular number concentration and

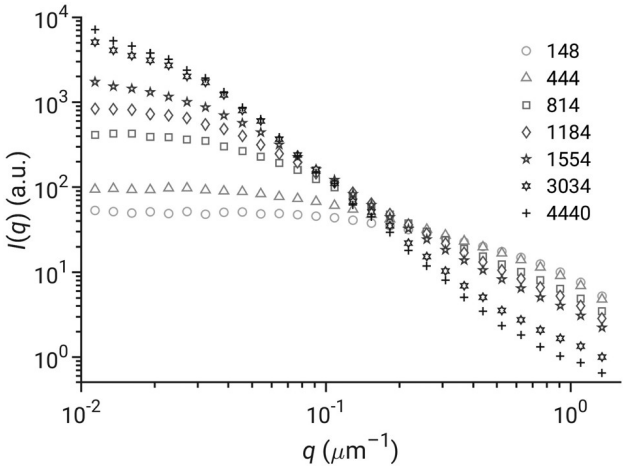

Fig. 5 Evolution of scattered light intensity *vs.* scattering vector magnitude for flocs obtained using 0.4 g L^{-1} alum with 400 μg L^{-1} *M. aeruginosa*. The q range of 0.1 to 0.5 μm^{-1} was used to determine the fractal dimension. Legend numbers indicate time (s).

size of the flocs present. The change, which was evident only in the $d_{0.9}$ and $D_{4,3}$ profiles but not in $d_{0.5}$ or $D_{3,2}$ [see Fig. S9(g), ESI†], indicates that the size evolution predominantly affected

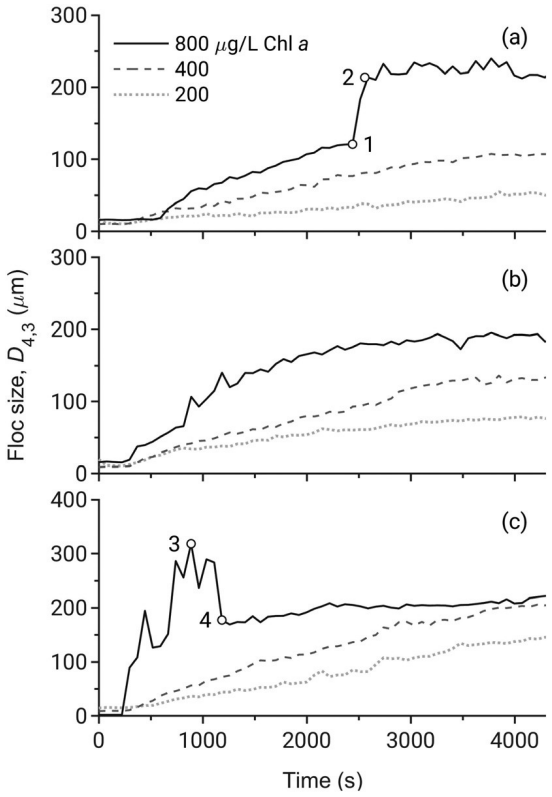

Fig. 6 Evolution of $D_{4,3}$ in *M. aeruginosa* cell suspensions with 200, 400, and 800 μg L^{-1} Chl *a* cell densities, flocculated with (a) 0.1 g L^{-1}, (b) 0.2 g L^{-1}, and (c) 0.4 g L^{-1} alum.

the larger end of the floc size distribution. The pronounced increase in these parameters suggests the sudden formation of a significant number of large flocs, likely resulting from the rapid aggregation of smaller flocs into much larger entities, leading to the presence of a relatively small population of large aggregates. Interestingly, the fractal dimension remained nearly constant at approximately 2.0 from point 1 to point 2, indicating that the overall structural complexity of the flocs did not change significantly despite the increase in their size.

At the highest alum concentration of 0.4 g L^{-1}, the trend was markedly different. The floc size initially surged to about 318 μm [point 3, Fig. 6(c)], followed by an eventual stochastic decrease to approximately 178 μm (point 4). During this period, the fractal dimension increased from around 1.7 at point 3 to about 2.0 at point 4. The absence of floc breakage in the early stages of flocculation, coupled with the rapid formation of porous flocs, led to the development of oversized flocs.[19] These oversized flocs subsequently experienced shear-induced fragmentation, resulting in a reduction in their size.

The final floc sizes (averages of last five data points, 4070–4366 s) are shown in Fig. 7. Even at the lowest alum concentration, the $D_{4,3}$ values of the flocs in the presence of alum were more than 13 times higher than those in the untreated 200 μg L^{-1} Chl *a M. aeruginosa* suspension and 5 times higher than those in the 800 μg L^{-1} Chl *a* cell suspension (*cf.* Fig. 7 and Table 1), indicating effective flocculation.

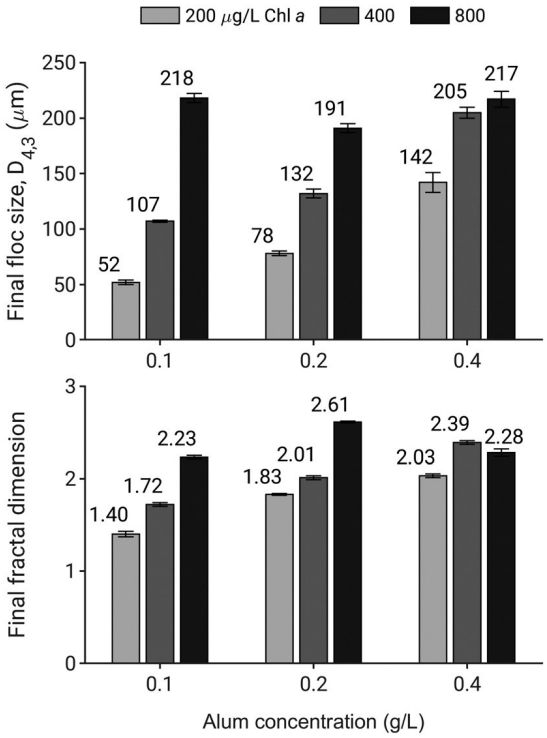

Fig. 7 Floc size and fractal dimension obtained with alum at $t \approx 4366$ s in *M. aeruginosa* suspensions of different cell densities.

Flocs formed in the 200 μg L^{-1} Chl *a* suspensions were relatively small ($D_{4,3} \lesssim 80$ μm) at alum concentrations of 0.1 and 0.2 g L^{-1}. However, increasing the coagulant dosage significantly affected floc size at both 200 and 400 μg L^{-1} Chl *a*. At 200 μg L^{-1} Chl *a*, $D_{4,3}$ increased from 52 μm to 78 μm and 142 μm with alum concentrations of 0.1, 0.2, and 0.4 g L^{-1}, respectively. A similar trend was observed at 400 μg L^{-1} Chl *a*, where $D_{4,3}$ values increased from 107 μm to 132 μm and 205 μm for the same alum concentrations.

In contrast, despite intermediate floc sizes being larger, the final floc sizes in the 800 μg L^{-1} Chl *a* cell suspensions remained similar across all alum concentrations, ranging between 205 ± 20 μm. The equilibrium aggregate size in orthokinetic flocculation is constrained by the balance between shear-induced floc formation and breakage,[19,34] with a specific upper limit influenced by shear rate and the bonding between particles in the floc mediated by the flocculant. Consequently, the final floc size of 205 ± 4 μm observed for 400 μg L^{-1} Chl *a* with 0.4 g L^{-1} alum was similar to the final $D_{4,3}$ values observed for the 800 μg L^{-1} Chl *a* suspensions, despite the latter having an estimated 43% higher primary particle concentration.

2.5 Floc size evolution using *M. oleifera* flocculant

Fig. 8(a) shows the $D_{4,3}$ evolution of the flocs in 200, 400, and 800 μg L^{-1} Chl *a* suspensions of *M. aeruginosa* in the presence of 2 mL L^{-1} of the deoiled *M. oleifera* seed extract. Floc sizes increased with cell density (number concentration), as expected. For a constant cell density of 800 μg L^{-1} Chl *a*, Fig. 8(b) shows that higher DMSE concentrations resulted in larger flocs.

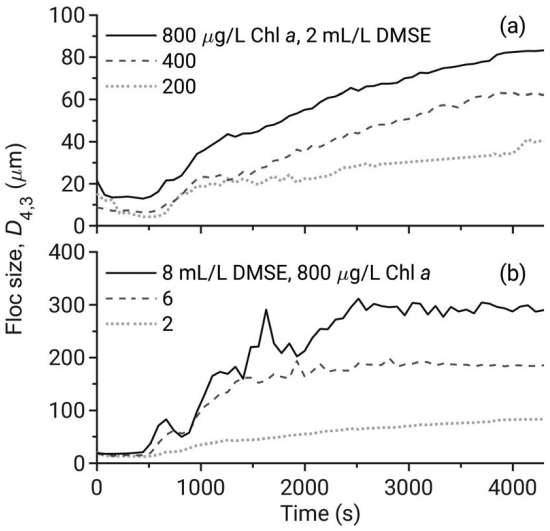

Fig. 8 Evolution of $D_{4,3}$ of the flocs in (a) 200, 400, and 800 μg L^{-1} Chl *a M. aeruginosa* cell suspensions flocculated using 2 mL L^{-1} DMSE, and (b) 800 μg L^{-1} Chl *a* cell suspensions flocculated using 2, 6, and 8 mL L^{-1} DMSE.

At the lowest concentration of 2 mL L^{-1}, DMSE showed limited effectiveness in promoting floc growth, especially at a cell concentration of 800 μg L^{-1} Chl *a* where the final floc size ($D_{4,3}$) was less than double that of the untreated suspension (*cf.* Fig. 9 and Table 1). However, at concentrations of 6 mL L^{-1} and 8 mL L^{-1}, DMSE proved significantly more effective, resulting in final $D_{4,3}$ values approximately 4 and 7 times larger, respectively, compared to the untreated suspension [Fig. 9(b)]. Furthermore, while the final floc size with alum was capped at about 218 ± 9 μm, it increased to 293 ± 6 μm with DMSE,

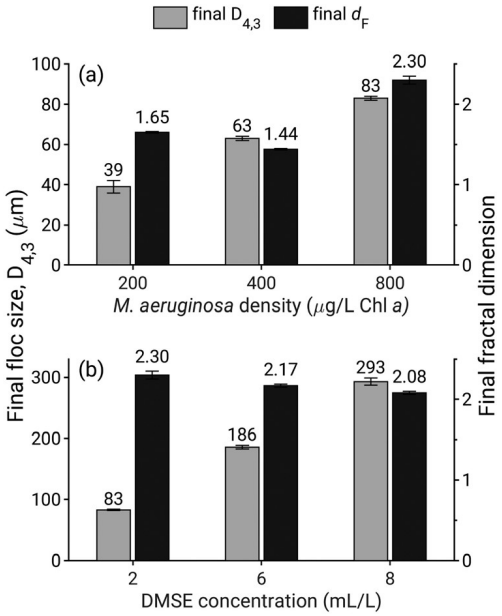

Fig. 9 Floc size and fractal dimension with DMSE at $t \approx 4366$ s: (a) effect of cell density at 2 mL L^{-1} DMSE; (b) effect of DMSE concentration at 800 μg L^{-1} Chl *a M. aeruginosa*.

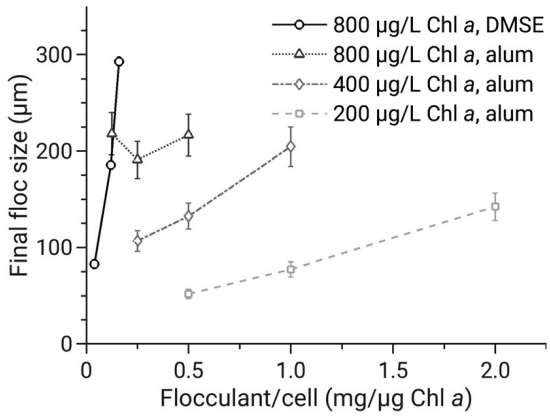

Fig. 10 Effect of flocculant dosage per unit of chlorophyll concentration (mg L^{-1} per μg L^{-1} Chl *a*) on the final floc size ($D_{4,3}$) for *M. aeruginosa* suspensions at different cell densities. The error bars represent 5% of the corresponding measured values.

indicating that DMSE can form flocs with greater shear resistance than alum.

2.6 Effect of flocculant dosage and algal concentration on final floc size

The final floc size is strongly influenced by both algal concentration and flocculant dosage. Fig. 10 depicts the relationship between flocculant amount (mg L^{-1}) per unit of chlorophyll (μg L^{-1} Chl *a*) and the resulting floc size. For DMSE, a protein concentration of 16 g L^{-1} (BSA equivalents) was used to calculate the flocculant/cell ratio.

In the case of alum, the final floc size increased with higher flocculant/cell ratios at algal concentrations of 200 and 400 μg L^{-1} Chl *a*. However, at 800 μg L^{-1} Chl *a*, the final floc size ($D_{4,3}$) reached a maximum of approximately 220 μm. In contrast, for DMSE, the final floc size attained was close to 300 μm, even at a significantly lower flocculant/cell ratio for the 800 μg L^{-1} Chl *a* suspensions. Throughout the range of DMSE concentrations tested, the final floc size demonstrated a much steeper dependence on DMSE concentration compared to alum, suggesting greater flocculant efficiency.

The reported $D_{4,3}$ values in Fig. 10 correspond to a flocculation time of 4366 s. It is expected that flocs will continue to grow until they reach a size that becomes unstable under the applied shear conditions. For the 800 μg L^{-1} Chl *a M. aeruginosa* suspensions, this stability limit was around 220 μm for alum and approximately 300 μm for DMSE. Beyond these sizes, further growth is less likely as the flocs become susceptible to shear-induced breakage.

2.7 Fractal dimension analysis of final *M. aeruginosa* flocs

The fractal dimensions of the final flocs (averages of d_F measured between 4070 and 4366 s of flocculation) ranged from about 1.40 (200 μg L^{-1} Chl *a M. aeruginosa* suspension with 0.1 g L^{-1} of alum) to 2.61 (800 μg L^{-1} Chl *a* suspension treated with 0.2 g L^{-1} alum). Lower d_F values were observed at lower cell densities or flocculant concentrations. Except for the

cases with 200 μg L^{-1} Chl *a* and 0.1 or 0.2 g L^{-1} alum, and 400 μg L^{-1} Chl *a* and 0.1 g L^{-1} alum, all experiments with alum resulted in final flocs with $d_F \gtrsim 2$. Similarly, experiments with 800 μg L^{-1} Chl *a* and DMSE yielded d_F values greater than 2.0.

The final d_F showed a moderate positive linear correlation with the final $D_{4,3}$ (correlation coefficient ≈ 0.59). Lower concentrations of alum and DMSE typically led to both lower d_F and smaller floc sizes. This trend was particularly evident in suspensions with 200 and 400 μg L^{-1} Chl *a M. aeruginosa* using 0.1 g L^{-1} alum and 2 mL L^{-1} DMSE, respectively, indicating that these concentrations were less effective in treating suspensions with low cell densities.

2.8 Floc structure evolution with alum and *M. oleifera* flocculants

Floc structure evolution was analyzed by examining the variation of d_F with $D_{4,3}$ during flocculation. Fig. 11 shows the evolution of d_F with $D_{4,3}$. In the initial phase ($t < 500$ s), d_F values below 1.0, derived from the $\log[I(q)]$ *vs.* $\log(q)$ data, indicated sparse aggregates and poorly formed flocs. As flocculation progressed, d_F increased, reflecting floc densification.

The d_F *vs.* $D_{4,3}$ profiles exhibit three distinct behaviors:

(1) Relatively smooth monotonic increase: d_F rises steadily with $D_{4,3}$ throughout the flocculation process, without major fluctuations. This suggests fast initial aggregation and ongoing internal rearrangement due to weak interparticle interactions. The increase in d_F could also be a consequence of break-up and re-formation, as discussed by Selomulya *et al.*[19]

(2) Leveling off: d_F stabilizes at a plateau, typically close to 2.1, within approximately 1000 s. This behavior indicates the early establishment of a stable floc structure, with floc growth proceeding alongside minimal structural changes over time.

(3) Stochastic increase: $D_{4,3}$ displays stochastic variations, characterized by significant fluctuations. By the end of the flocculation process, d_F shows an overall upward trend. These variations may stem from either reaction- or diffusion-limited aggregation mechanisms, coupled with structural densification.

These behaviors highlight the dynamic nature of floc formation influenced by the aggregation/fragmentation dynamics and internal structural changes over time, as further exemplified below.

Case 1: using alum with *M. aeruginosa* suspensions at cell densities of 200 and 400 μg L^{-1} Chl *a*, caused the fractal dimension to increase continuously with floc size. The d_F *vs.* $D_{4,3}$ profiles for these two cell densities were nearly identical for a given alum concentration, though both final d_F and $D_{4,3}$ values were higher for the 400 μg L^{-1} Chl *a* suspension compared to the 200 μg L^{-1} Chl *a* suspension [*cf.* Fig. 11(a)–(c)]. The highest fractal dimension observed at these lower cell densities was ≈ 2.39, corresponding to the highest concentration of alum used in the study (0.4 g L^{-1}). The monotonic increase in d_F was generally a feature of alum-based flocculation at low and intermediate cell densities. However, a similar continuous increase in the fractal dimension was observed with 2 mL L^{-1} DMSE, as shown in Fig. 11(d).

Case 2: with the *Moringa* extract at concentrations of 6 or 8 mL L^{-1} and *M. aeruginosa* at 800 μg L^{-1} Chl *a* cell density, d_F initially increased and then remained almost constant as floc growth continued [*cf.* Fig. 11(e)]. In these cases, d_F reached a plateau value of 2.1 ± 0.2 within about 1000 s of the flocculation process. $D_{4,3}$ continued to increase.

Case 3: using 0.4 g L^{-1} alum with 800 μg L^{-1} Chl *a* *M. aeruginosa* initially led to rapid floc growth to 318 μm with $d_F = 1.7$ [point 3 in Fig. 11(c)], indicating diffusion-limited aggregation,[25–27] followed by breakdown to 178 μm (point 4). Subsequently, flocs grew again to 215 μm with $d_F \approx 2.3$.

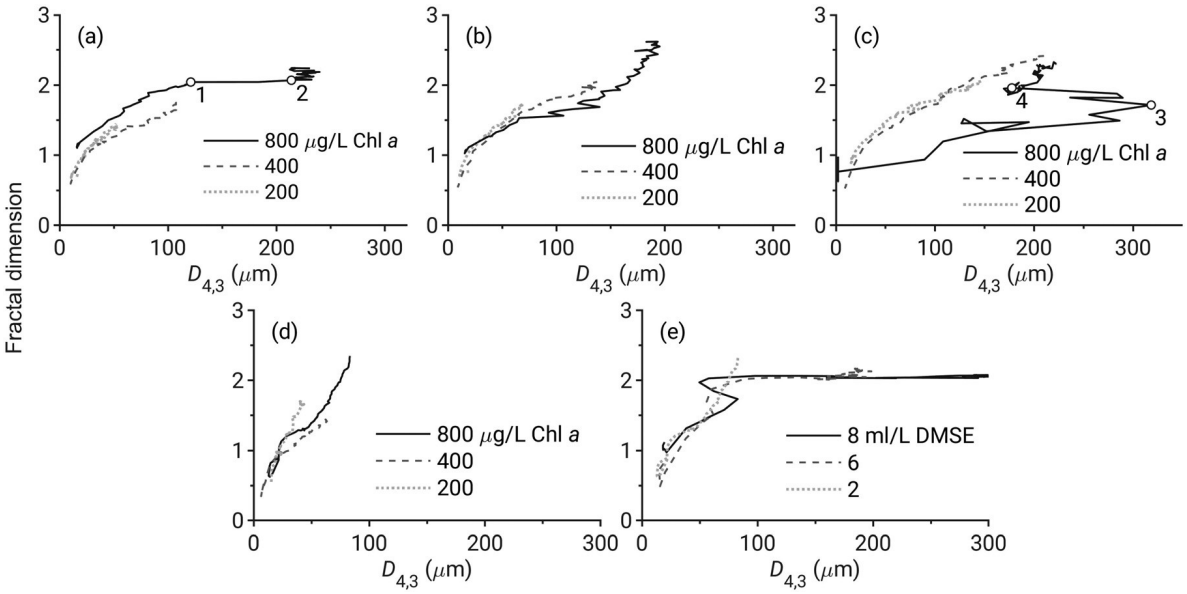

Fig. 11 Fractal dimension of *M. aeruginosa* flocs *vs.* floc size for different cell densities and alum/DMSE concentrations: (a) 0.1 g L^{-1} alum, (b) 0.2 g L^{-1} alum, (c) 0.4 g L^{-1} alum, (d) 2 mL L^{-1} DMSE with varying cell densities, (e) 800 μg L^{-1} Chl *a* with varying DMSE concentrations.

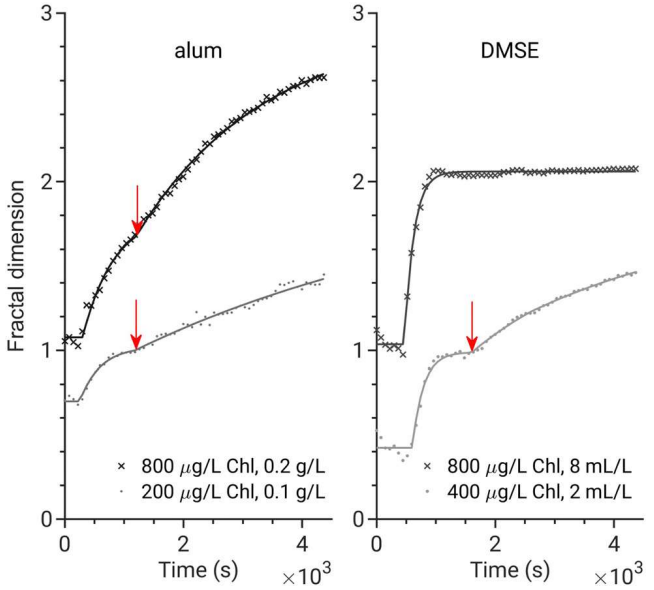

Fig. 12 Fractal dimension of *M. aeruginosa* flocs over time. Symbols represent experimental data and curves are fits based on eqn (6), with a time delay included for the induction period [*cf.* eqn (S3), ESI†]. Arrows indicate time t_1, marking the end of the initial phase of increase in d_F and the start of the second phase of increase.

At 0.1 g L^{-1} alum and the same cell density, flocs steadily grew to 121 μm with $d_F \approx 2.04$ [point 1 in Fig. 11(a)], and then aggregated suddenly to 214 μm (point 2) with minimal change in d_F.

Fig. 12 presents the d_F profiles over time for selected flocculation experiments, comparing alum and *M. oleifera* as flocculants. Data for other experiments are in Fig. S14 (ESI†). Alum consistently showed a continuous increase in d_F with time, indicating floc structural rearrangement throughout the process. The rate of increase in d_F due to restructuring has been modeled as

$$\frac{dd_F}{dt} = k(d_{F,max} - d_F) \quad (6)$$

where $d_{F,max}$ is the maximum attainable value of d_F in a given system.[19,22] In general, the rate constant, k, is influenced by factors such as floc size, but treating it as an empirical constant has also yielded good fits to experimental data. Eqn (S3) (ESI†) gives the integrated form of the rate equation that models the asymptotically exponential growth of d_F with time.

The alum data showed three distinct regions: an induction period lasting up to $t_0 = 7 \pm 3$ min, followed by an asymptotic increase in d_F up to $t_1 = 17 \pm 4$ min (indicated by arrows in Fig. 12), and a subsequent phase where d_F continued to increase at a slower rate, approaching $d_{F,max}$. Initially, the fractal dimension increased from $d_{F,0}$ to an intermediate value, $d_{F,1}$ at $t = t_1$, and then continued to increase due to slower densification. For the various cell densities and alum concentrations, $d_{F,1}$ ranged from about 1.0 to 1.8, approximated by $d_{F,1} = 0.85 + 8.56 \times 10^{-4}x_1 + 0.6x_2$, where x_1 is the cell density in μg L^{-1} Chl *a* and x_2 is the alum concentration in g L^{-1}.

The rate constants, k_1, for the initial increase from $d_{F,0}$ to $d_{F,1}$ were in the range 0.19 ± 0.08 min^{-1}, and those for the subsequent rise, k_2, were significantly lower, in the range 0.03 ± 0.02 min^{-1}.

Similar trends were observed with DMSE at a concentration of 2 mL L^{-1} and with 200, 400, and 800 μg L^{-1} Chl *a* cell densities. After an induction period lasting up to $t_0 = 12 \pm 2$ min, d_F increased at an asymptotically exponential rate of $k_1 = 0.41 \pm 0.9$ min^{-1} reaching $d_{F,1} = 1.1 \pm 0.2$ at $t_1 = 30 \pm 3$ min. Although the induction period was somewhat longer, the initial rate constant, k_1, was higher with DMSE compared to alum. This was followed by continued growth with rate constant, k_2, in the 0.03 ± 0.01 min^{-1} range, similar to the densification rate constants observed in experiments using alum.

In contrast to all alum concentrations and the lower DMSE concentration, higher concentrations of 6 and 8 mL L^{-1} DMSE rapidly increased d_F to $\approx 2.1 \pm 0.1$ within the first 20 min of flocculation at a rate of 0.32 ± 0.06 min^{-1}, after which d_F remained steady. As seen in Fig. 11(e), d_F stayed almost unchanged even though the floc size continued to increase.

It is interesting to compare the slower rate of floc growth observed with 0.2 g L^{-1} alum to the faster rate observed with 8 mL L^{-1} DMSE, both in 800 μg L^{-1} Chl *a* cell suspension (*cf.* Fig. 12). Despite the slower rate with alum, the final fractal dimension achieved at the end of ≈73 min was higher (2.61 compared to 2.08). However, the final floc size was significantly larger with DMSE (293 μm compared to 191 μm). Similarly, with 2 mL L^{-1} DMSE and 800 μg L^{-1} Chl *a* cell density, although the final fractal dimension was higher (2.30), the final $D_{4,3}$ was only 83 μm (*cf.* Fig. 9).

3 Conclusions

In summary, this study investigated the fractal dynamics of *M. aeruginosa* flocs under varying concentrations of flocculant and *M. aeruginosa* cell density. Significant differences in floc size and fractal dimension evolution were observed between DMSE and alum as flocculants.

With 6 and 8 mL L^{-1} of DMSE, d_F initially increased rapidly, reaching a plateau within about 20 min of flocculation. On the other hand, alum exhibited a slower two-phase floc structure growth pattern across all conditions. At the lower DMSE dosage of 2 mL L^{-1}, the evolution characteristics of the floc structure resembled those observed with alum.

The key difference between alum and DMSE was in how they affected the evolution of fractal dimensions with floc size. At comparable mass concentrations, alum's higher molar concentration and charge density would enhance its charge neutralization ability. Therefore, alum induced rapid, diffusion-controlled flocculation, producing porous flocs with initially lower fractal dimensions. Weak interparticle interactions allowed internal restructuring, gradually increasing fractal dimensions over time. In contrast, the polymeric nature of the *M. oleifera* flocculant, and the patch charge and possibly bridging interactions it mediates, hindered the restructuring of the aggregates. Additionally, the adsorption steps involving *M. oleifera* macromolecules would be slower compared to alum. As a result, DMSE as a flocculant led to the early attainment of relatively high fractal dimensions, which remained stable as the flocs continued to grow. Notably, a lower

dosage of 2 mL L^{-1} was insufficient for generating stable flocs resistant to restructuring and fragmentation; higher concentrations of 6 or 8 mL L^{-1} DMSE were necessary.

With alum, d_F continued to increase throughout 73 min of flocculation, beyond the maximum value attained with DMSE. Higher cell densities and increased alum concentrations initially led to larger flocs, but these eventually fragmented into smaller ones due to shear-induced breakage, establishing an upper limit on $D_{4,3}$. In contrast, final floc diameters achieved with DMSE exceeded this upper limit observed with alum, highlighting DMSE's superior floc strength. Despite alum resulting in flocs with higher fractal dimensions at the end ($t \approx 73$ min), DMSE produced larger and more resilient flocs. Specifically, DMSE, applied at 8 mL L^{-1} (equivalent to $\approx$0.128 g L^{-1} protein), produced larger final floc sizes (293 $\pm$ 6 μm) compared to alum at 0.2 g L^{-1} (191 $\pm$ 5 μm) in 800 μg L^{-1} Chl *a M. aeruginosa* suspensions.

Furthermore, floc strength was notably low in 400 μg L^{-1} *M. aeruginosa* suspensions treated with 0.1, 0.2, and 0.4 g L^{-1} alum. When subjected to an increased stirring speed of 250 rpm, floc sizes in these suspensions, initially ranging in $D_{4,3}$ from approximately 107 to 205 μm at 70 rpm, converged to a nearly same value of 73 $\pm$ 3 μm (almost independent of alum concentration). This observation suggests a significant impact of shear on floc stability, warranting further investigation into the relationship between shear and floc strength.

4 Materials and methods

4.1 Materials

Microcystis aeruginosa (UTEX LB 2385 strain, sourced from Little Rideau Lake, Ontario) was obtained from the UTEX Culture Collection of Algae (University of Texas, Austin). The growth medium, BG-11 powder, was purchased from Phyto-Technology Laboratories (B1511, Shawnee Mission, KS). *Moringa oleifera* seeds were purchased from NatureVibe (India). Alum [$KAl(SO_4)_2 \cdot 12H_2O$, Wards Science, VWR], sodium chloride (Fisher Chemical), ethanol (95% v/v Pharmco-Aaper), acetone (>99.5%, VWR), bovine serum albumin (BSA, Biotechnology Grade, Amresco, Solon, OH), and Biuret protein assay reagent (M262, VWR) were used as received.

4.2 Methods

Algal culture. The *M. aeruginosa* strain was cultured in sterile BG-11 medium, prepared by dissolving 1.68 g L^{-1} of BG-11 in deionized water. The medium was sterilized by autoclaving at 121 °C for 20 min. Cultures were maintained at room temperature under a 12 h light:12 h dark photoperiod, following the procedure reported by Bortoli *et al.*[35] Cell density of the suspensions was quantified in terms of chlorophyll *a* concentration using a fluorometer at an excitation wavelength of 430 nm and an emission wavelength of 680 nm. An aliquot of the cell suspension was vacuum-filtered using a polycarbonate membrane (Isopore) with a 0.2 μm pore size. The filter and retentate were placed into a 15 mL amber-colored polypropylene tube, and 10 mL of 90% acetone was added. The tube was capped and kept in the dark at 4 °C for 12 h to extract Chl *a* in acetone. The Chl *a* concentration in the extract was determined using the Welschmeyer method.[36] When the original cell suspension needed dilution before filtration (to ensure the measurement was within the fluorometers range), this dilution was factored in accordingly. The pH and conductivity measurements were performed using an Oakton PC 450 benchtop meter. Optical microscopy images were acquired using a Nikon Eclipse L200N microscope.

***M. oleifera* seed protein extraction.** Water extracts of the *M. oleifera* seeds were prepared according to the procedure reported by Kalibbala *et al.*[37] The seed husk was broken, and the seeds unshelled (see Fig. S1, ESI†). The dehusked seeds were ground to a powder form using a kitchen grinder to a size of $d_{0.5} \approx 90$ μm and $d_{0.9} \approx 200$ μm. The seed powder (5.0 g) was extracted with 95% ethanol (100 mL). The mixture was magnetically stirred for 30 min, after which the liquid phase was separated by centrifugation at 3400 rpm for 10 min (Labnet Hermle Z206A centrifuge). The supernatant was decanted, and the settled powder was dried on a glass Petri dish for about 24 h, yielding approximately 3.64 g of deoiled seed powder. This powder was combined with another similarly prepared batch.

The deoiled seed powder (5.0 g) was further extracted with 1 M aqueous NaCl solution (100 mL) for 30 min with a magnetic stirrer. The dispersion was then vacuum-filtered through a 5-μm filter (VWR, Grade 413) and filtered again using a syringe filter (Millex, MilliporeSigma) of the same pore size before use in the light scattering experiments for studying *M. aeruginosa* flocculation.

Extract protein concentration and surface tension measurements. The Biuret assay, utilizing BSA as the standard, was employed to analyze the protein concentration in the seed extract. Detailed procedures are outlined in Section S2 (ESI†). At 280 nm, the extinction coefficient of the protein extract was determined to be 0.74 $\pm$ 0.03 L g^{-1} cm^{-1}. Protein concentrations of DMSE samples were then calculated in BSA equivalents based on their absorbance at 280 nm. Surface tensions were measured at room temperature using a bubble tensiometer (SITA Dyno-Tester) after diluting DMSE to various concentrations (ranging from 0.005 to 10 g L^{-1}) using 1 M aqueous NaCl solution.

Light scattering analysis of flocculation kinetics. Three different concentrations of *M. aeruginosa* cell suspensions were used in the flocculation studies. The cell culture ($\approx$2000 μg L^{-1} Chl *a* cell density) was diluted to concentrations of 200, 400, and 800 μg L^{-1} Chl *a* using deionized water. Alum and DMSE were used as the flocculants. Light scattering analysis was performed using Mastersizer 2000 (Malvern Instruments, UK), with a 633 nm He–Ne laser of 0.63 mm beam diameter and 1.5 mrad beam divergence as the light source and a 44-channel detector array for measuring the intensity of the scattered light at scattering angles in the range of $\approx$0.02 to 60°. A Hydro 2000S dispersion unit was used to mix the fluid, preventing particle settling while continuously recirculating it through the flow cell for light scattering analysis. It comprised of a tank of 150-mL capacity and an agitator shaft with an impeller at the bottom to pump the fluid out of the dispersion unit into the flow cell.

About 100 mL of the cell suspension was poured into the dispersion chamber of Hydro 2000S, and a measured amount of the flocculant (in the range of 10 to 40 mg of alum and 0.2 to 0.8 mL of DMSE) was added. The impeller rotational speed was set to an initial high value of 1050 rpm for 20 s, after which the speed was decreased to 70 rpm, and the data collection was started.

The volume-weighted mean diameter, $D_{4,3}$, and the surface-weighted mean, $D_{3,2}$, diameter were calculated from the volume distribution (volume v_i of particles with diameter d_i) using

$$D_{m,n} = \left[\frac{\sum_i v_i d_i^{m-3}}{\sum_i v_i d_i^{n-3}}\right]^{\frac{1}{m-n}} \quad (7)$$

$d_{0.5}$ and $d_{0.9}$ represent the median and the 90th percentile diameters, respectively.

Obscuration (Ob) measures the light intensity extinction caused by a sample in the light beam's path. It is defined by

$$\mathrm{Ob} = 1 - \frac{I_s}{I_b} \quad (8)$$

where I_s is the light intensity at the central detector with the sample present and I_b is without particles (neat dispersant). Theoretical calculation of obscuration uses

$$\mathrm{Ob} = 1 - e^{-\alpha_{ext} b} \quad (9)$$

with α_{ext} as the attenuation coefficient, and b, the light's path length. $\alpha_{ext,i}$ for particles of diameter d_i and number concentration, n_i, is given by

$$\alpha_{ext,i} = Q_{ext,i}\left(\frac{\pi d_i^2}{4}\right) n_i \quad (10)$$

where the efficiency of light extinction by scattering and absorption, $Q_{ext,i} = Q_{sca,i} + Q_{abs,i}$, is derived from Mie theory.[38]

For a distribution of n_i particles of diameter d_i

$$\alpha_{ext} = \sum_i Q_{ext,i}\left(\frac{\pi d_i^2}{4}\right) n_i \quad (11)$$

For identical diameter, d,

$$\alpha_{ext} = \frac{\pi}{4} Q_{ext} d^2 N \quad (12)$$

where N is total particle concentration. Eqn (9) and (12) yield:

$$\mathrm{Ob} = 1 - \exp\left(-\frac{\pi}{4} Q_{ext} d^2 N b\right) \quad (13)$$

The number density of cells in the dispersion can be determined using the following rearranged equation

$$N = -\frac{4\ln(1 - \mathrm{Ob})}{\pi Q_{ext} d_p^2 b} \quad (14)$$

allowing for quantification of cellular concentration based on the measured obscuration and the optical properties of the system.

Data availability

The analyzed datasets discussed herein are included in this article and its ESI.†

Conflicts of interest

There are no conflicts to declare.

Acknowledgements

This research was supported by the New York State Center of Excellence in Healthy Water Solutions (Award C190175). The use of experimental facilities at the Center for Advanced Materials Processing, a New York State Center for Advanced Technology at Clarkson University, is also acknowledged. The authors thank Dr Michael Twiss for his guidance in determining the chlorophyll *a* concentrations in *M. aeruginosa* suspensions.

Notes and references

1 E. J. Summers and J. L. Ryder, *J. Environ. Manage.*, 2023, **330**, 117141.
2 K. Foreman, D. Vacs Renwick, M. McCabe, A. Cadwallader, H. Holsinger, C. Kormondy and R. Albert, *AWWA Water Sci.*, 2021, **3**, e1223.
3 A. Jain, R. Subramanian, B. Manohar and C. Radha, *J. Food Sci. Technol.*, 2019, **56**, 2093–2104.
4 A. Ndabigengesere, K. S. Narasiah and B. G. Talbot, *Water Res.*, 1995, **29**, 703–710.
5 U. Gassenschmidt, K. D. Jany, T. Bernhard and H. Niebergall, *Biochem. Biophys. Acta*, 1995, **1243**, 477–481.
6 M. Moulin, E. Mossou, L. Signor, S. Kieffer-Jaquinod, H. M. Kwaambwa, F. Nermark, P. Gutfreund, E. P. Mitchell, M. Haertlein, V. T. Forsyth and A. R. Rennie, *J. Colloid Interface Sci.*, 2019, **554**, 296–304.
7 L. Brennan and P. Owende, *Renewable Sustainable Energy Rev.*, 2010, **14**, 557–577.
8 S. B. Kurniawan, S. R. S. Abdullah, M. F. Imron, N. S. M. Said, N. Ismail, H. A. Hasan, A. R. Othman and I. F. Purwanti, *Int. J. Environ. Res. Public Health*, 2020, **17**, 9312.
9 W. Yuheng, Z. Shengguang, L. Na and Y. Yixin, *Procedia Environ. Sci.*, 2011, **8**, 75–80.
10 F. Sun, H.-Y. Pei, W.-R. Hu and C.-X. Ma, *Chem. Eng. J.*, 2012, **193**, 196–202.
11 D. Kyung, D. Kim, N. Park and W. Lee, *J. Environ. Manage.*, 2013, **131**, 74–81.
12 B. D. Arbo, L. E. Schimith, M. Goulart dos Santos and M. A. Hort, *Eur. J. Pharmacol.*, 2022, **919**, 174800.
13 M. Saleem and R. T. Bachmann, *J. Ind. Eng. Chem.*, 2019, **72**, 281–297.
14 S. Y. Choy, K. M. N. Prasad, T. Y. Wu, M. E. Raghunandan and R. N. Ramanan, *J. Environ. Sci.*, 2014, **26**, 2178–2189.
15 N. A. Oladoja and G. Pan, *Sustainable Chem. Pharm.*, 2015, **2**, 37–43.

16 F. P. Camacho, V. S. Sousa, R. Bergamasco and M. Ribau Teixeira, *Chem. Eng. J.*, 2017, **313**, 226–237.
17 M. G. Rasteiro and A. Koponen, *Powders*, 2024, **3**, 77–110.
18 R. K. Chakraborti, K. H. Gardner, J. F. Atkinson and J. E. Van Benschoten, *Water Res.*, 2003, **37**, 873–883.
19 C. Selomulya, G. Bushell, R. Amal and T. Waite, *Chem. Eng. Sci.*, 2003, **58**, 327–338.
20 M. Lattuada, H. Wu, P. Sandkühler, J. Sefcik and M. Morbidelli, *Chem. Eng. Sci.*, 2004, **59**, 1783–1798.
21 E. Antunes, F. A. P. Garcia, P. Ferreira, A. Blanco, C. Negro and M. G. Rasteiro, *Ind. Eng. Chem. Res.*, 2008, **47**, 6006–6013.
22 E. Antunes, F. Garcia, P. Ferreira, A. Blanco, C. Negro and M. Rasteiro, *Chem. Eng. Sci.*, 2010, **65**, 3798–3807.
23 A. Metaxas, N. Wilkinson, E. Raethke and C. S. Dutcher, *Soft Matter*, 2018, **14**, 8627–8635.
24 W. B. Russel, D. A. Saville and W. R. Schowalter, *Colloidal Dispersions*, Cambridge University Press, Cambridge, 1989.
25 G. Pranami, M. H. Lamm and R. D. Vigil, *Phys. Rev. E: Stat., Nonlinear, Soft Matter Phys.*, 2010, **82**, 051402.
26 J. Liu, W. Y. Shih, M. Sarikaya and I. A. Aksay, *Phys. Rev. A: At., Mol., Opt. Phys.*, 1990, **41**, 3206–3213.
27 P. Meakin, *J. Colloid Interface Sci.*, 1984, **102**, 505–512.
28 M. M. Özcan, *S. Afr. J. Bot.*, 2020, **129**, 25–31.
29 S. Andrews, D. Nover and S. G. Schladow, *Limnol. Oceanogr.: Methods*, 2010, **8**, 507–526.
30 N.-T. Le, J. M. Myrick, T. Seigle, P. T. Huynh and S. Krishnan, *Adv. Powder Technol.*, 2018, **29**, 3007–3021.
31 J. J. Cole, S. Findlay and M. L. Pace, *Mar. Ecol.: Prog. Ser.*, 1988, **43**, 1–10.
32 World Health Organization, Guidelines for safe recreational water environments. Volume 1, Coastal and fresh waters, 2003, Available at **https://iris.who.int/handle/10665/42591** (accessed July 2024).
33 T. Chatsungnoen and Y. Chisti, *Algal Res.*, 2016, **13**, 271–283.
34 A. Blanco, E. Fuente, C. Negro and J. Tijero, *Can. J. Chem. Eng.*, 2002, **80**, 1–7.
35 S. Bortoli, D. Oliveira-Silva, T. Krüger, F. A. Dörr, P. Colepicolo, D. A. Volmer and E. Pinto, *Rev. Bras. Farmacogn.*, 2014, **24**, 389–398.
36 N. A. Welschmeyer, *Limnol. Oceanogr.*, 1994, **39**, 1985–1992.
37 H. Kalibbala, O. Wahlberg and T. Hawumba, *Water Sci. Technol.: Water Supply*, 2009, **9**, 707–714.
38 C. F. Bohren and D. R. Huffman, *Absorption and Scattering of Light by Small Particles*, John Wiley & Sons, 1983.

Supplementary Information

Light Scattering Study of Algal Floc Growth and Structure: Alum vs. Polymeric Plant-Derived Flocculant

Temitope Orimolade[a], Ngoc-Tram Le[a], Lyle Trimble[a], Bandaru V. Ramarao[b], and Sitaraman Krishnan[a,*]

[a]Department of Chemical & Biomolecular Engineering, Clarkson University, 8 Clarkson Avenue, Potsdam, New York 13699, USA

[b]Department of Chemical Engineering, SUNY College of Environmental Science & Forestry, 1 Forestry Drive, Syracuse, New York 13210, USA

*Corresponding author. Email: skrishna@clarkson.edu, Phone: +1 315 268 6661

Contents

S1 *Moringa oleifera* seed proteins

The low molecular weight, high charge-density cationic proteins from *Moringa oleifera* seeds, specifically MO2 and Mo-CBP3 (a 2S albumin), are effective flocculants for negatively charged particles. Their high arginine content, approximately 11.7%, significantly enhances this activity (see Table S1).

Table S1: Amino acid compositions of *M. oleifera* proteins

	MO2		**CBP3**	
Amino acid	#	%	#	%
Alanine	2	3.33	11	6.75
Cysteine	2	3.33	8	4.91
Aspartic acid	1	1.67	8	4.91
Glutamic acid	0	0.00	11	6.75
Phenylalanine	1	1.67	3	1.84
Glycine	5	8.33	6	3.68
Histidine	1	1.67	2	1.23
Isoleucine	2	3.33	6	3.68
Lysine	0	0.00	1	0.61
Leucine	3	5.00	15	9.20
Methionine	1	1.67	4	2.45
Asparagine	2	3.33	4	2.45
Proline	7	11.67	11	6.75
Glutamine	15	25.00	25	15.34
Arginine	7	11.67	19	11.66
Serine	4	6.67	8	4.91
Threonine	2	3.33	7	4.29
Valine	4	6.67	11	6.75
Tryptophan	0	0.00	1	0.61
Tyrosine	1	1.67	2	1.23
Total	60		163	
Molecular wt. (g/mol)	6782		18756	
Theoretical pI	11.61		7.55	

The amino acid sequence of the MO2 proteins is,[1]

> QGPGRQPDFQ RCGQQLRNIS PPQRCPSLRQ AVQLTHQQQG QVGPQQVRQM YRVASNIPST

and that of the 2S albumin CBP3 chitin-binding protein is,[2]

MAKLTLLLAT LALLVLLANA SIYRTTVELD EEPDDNQQQR CRHQFQTQQR LRACQRVIRR WSQGGGPMED VEDEIDETDE IEEVVEPDQA RRPPTLQRCC RQLRNVSPFC RCPSLRQAVQ SAQQQQGQVG PQQVGHMYRV ASRIPAICNL QPMRCPFRQQ QSS

The isoelectric point of MO2 is about 11.6. Both proteins are rich in glutamine (≈ 25.0% in MO2 and 15.3% in CBP3) and share a common glutamine-rich peptide sequence (QQQGQVG-PQQV) (highlighted in blue). They also contain significant amounts of nonpolar proline (approximately 11.7% in MO2 and 6.8% in CBP3).

S2 Properties of *M. oleifera* seed extract

Fig. S1: Photographs of (a) whole, (b) dehusked, and (c) powdered *Moringa oleifera* seeds, along with (d) the aqueous extract.

While powdered *M. oleifera* seeds are effective as flocculants, their use can increase organic matter in treated water, potentially promoting microorganism growth.[3] The seeds contain about 40% oils, 40% proteins, and 10% carbohydrates.[4] Deoiling the seeds or extracting the active flocculant can reduce the organic matter added during treatment. Several studies have explored extracting coagulation-active proteins using aqueous salt solutions.[5–7] Ndabigengesere et al.[5] found that only water extracts of *M. oleifera* seeds possess coagulation activity, while extracts using petroleum ether, hexane, chloroform, acetone, and methanol do not. Oladoja et al.[8] extracted seed proteins using aqueous NaCl solution, precipitated them with ammonium sulfate, and found that the precipitate, combined with soil (sand and clay), was an effective flocculant for *M. aeruginosa*, although a large amount of ammonium sulfate—six times the seed mass—was required in processing the seeds. Camacho et al.[9] studied the effectiveness of *M. oleifera* seed powders in three forms for cyanobacteria removal: untreated seed powder, oil-extracted using propane at 30 °C and 80 bar (reducing oil content by 94%), and oil-extracted using 95% ethanol (reducing oil content by 76%). They found that low-turbidity waters required the extraction of the active ingredient for effective turbidity reduction, which was not necessary for high-turbidity water. Madrona et

al.[10] compared the flocculation activity of *M. oleifera* proteins extracted using various KCl concentrations down to 0.01 M. Best results were with 1 M KCl, likely due to increased ionic strength enhancing protein concentration in the extract via the salting-in mechanism.[7,11] In this study, *M. oleifera seeds* were deoiled using 95% ethanol, and the seed proteins were extracted in 1 M aqueous NaCl solution.

Spectroscopic determination of M. oleifera protein concentration

Standard solutions of bovine serum albumin (BSA) with nominal concentrations of 0, 2, 4, 6, and 8 g/L were prepared by serial dilution of a 10 g/L BSA solution in aqueous NaCl (9 g/L). Their UV-vis spectra were recorded [see Fig. S2(a)]. The absorbance peak near 280 nm increased linearly with protein concentration up to about 6 g/L (data not shown). The BSA concentrations were corrected using the 280-nm absorbance and the known extinction coefficient of 0.667 $(\text{mg/mL})^{-1}\text{cm}^{-1}$.[12]

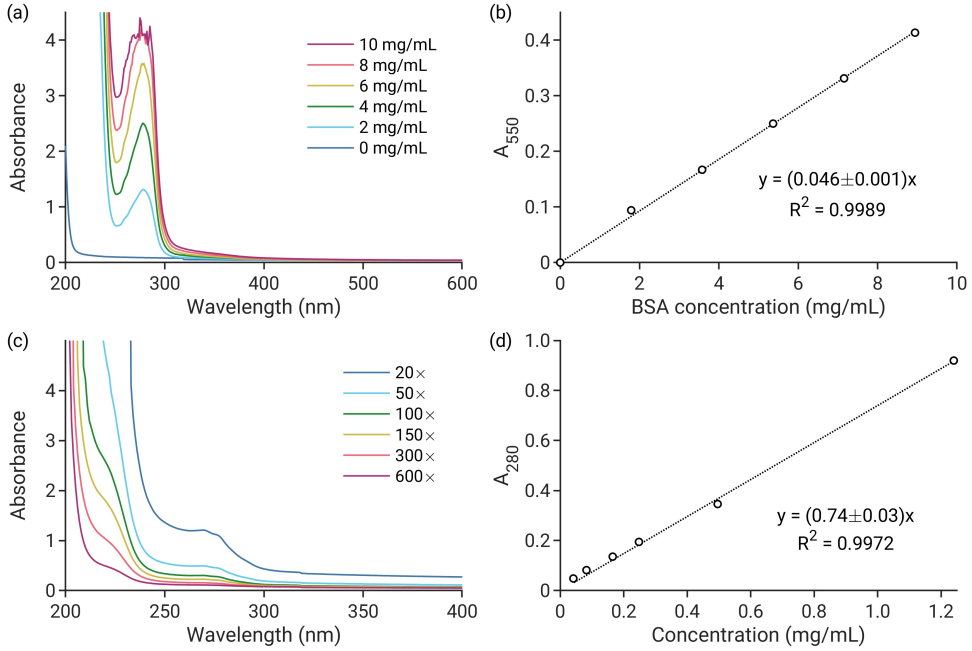

Fig. S2: (a) UV-vis spectra of BSA solutions in 0.9% aqueous NaCl with nominal concentrations ranging from 0 to 10 mg/mL protein. (b) Absorbance at 550 nm of BSA solution (1 mL) and Biuret reagent (4 mL). (c) UV-vis spectra of *M. oleifera* seed extracts in 1 M aqueous NaCl at various dilutions. (d) Absorbance at 280 nm of the *M. oliefera* extracts as a function of concentration (in BSA equivalents).

Next, a Biuret assay was conducted by adding 4 mL of Biuret reagent (Protein Assay Reagent M262, VWR) to 1 mL of each BSA standard, followed by vortexing and a 20-min incubation at room temperature. Absorbance at 550 nm was measured, with 9 g/L saline as the blank.

The plot of A_{550} vs. BSA concentration showed good linearity [see Fig. S2(b)], yielding an extinction coefficient ε_{550} of 0.046 ± 0.001 $(\mathrm{mg/mL})^{-1}\mathrm{cm}^{-1}$.

The Biuret assay was also applied to 1 mL of neat *M. oleifera* seed extract with 4 mL of Biuret reagent. The BSA equivalent concentration was derived from the calibration curve [Fig. S2(b)], resulting in 16 ± 2 mg/mL in the deoiled *Moringa* seed extract (DMSE).

Finally, by measuring the absorbance of diluted *M. oleifera* seed extract in 1 M NaCl solution, an extinction coefficient ε_{280} of 0.74 $(\mathrm{mg/mL})^{-1}\mathrm{cm}^{-1}$ for the *M. oleifera* protein was determined [Fig. S2(c) and (d)]. This coefficient could be used to calculate protein concentration in *M. oleifera* extracts from a single absorbance measurement at 280 nm, following suitable dilution.

Surface tension of M. oleifera seed extract

Fig. S3 shows the effect of *M. oleifera* protein concentration (in BSA equivalents) on the surface tension of the solution. The dependence of surface tension, γ (mN/m), on concentration, c (g/L), could be empirically fitted to an equation of the form:

$$\gamma = \gamma_0 - p_1 \ln\left(1 + p_2 c\right) \tag{S1}$$

The values of the parameters γ_0, p_1, and p_2 are shown in Fig. S3.

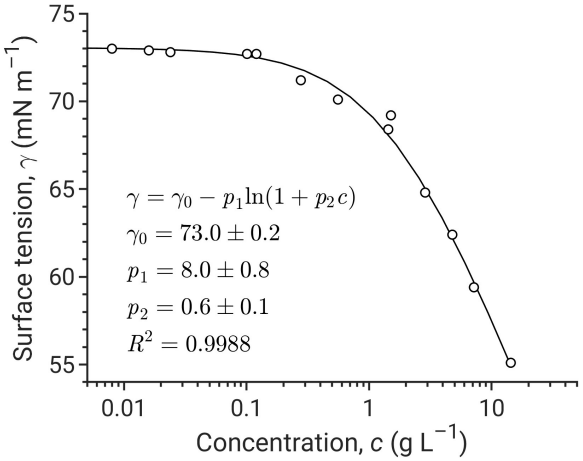

Fig. S3: Surface tension versus concentration of the active ingredient in the extracts of deoiled *M. oleifera* seeds in 1 M aqueous NaCl at 23.5 °C.

S3 Size distribution in *M. aeruginosa* suspensions at different cell concentrations

Fig. S4 shows the size distribution of *M. aeruginosa* cells in suspensions of three different concentrations. Flocculation of the cells is evident even without adding a flocculant. The flocs remained relatively stable at 70 rpm. In the 200 μg/L Chl *a* suspension, the flocs stabilized after a small decrease in size, whereas those in the 800 μg/L Chl *a* suspension showed a slight increase due to shear-induced aggregation.

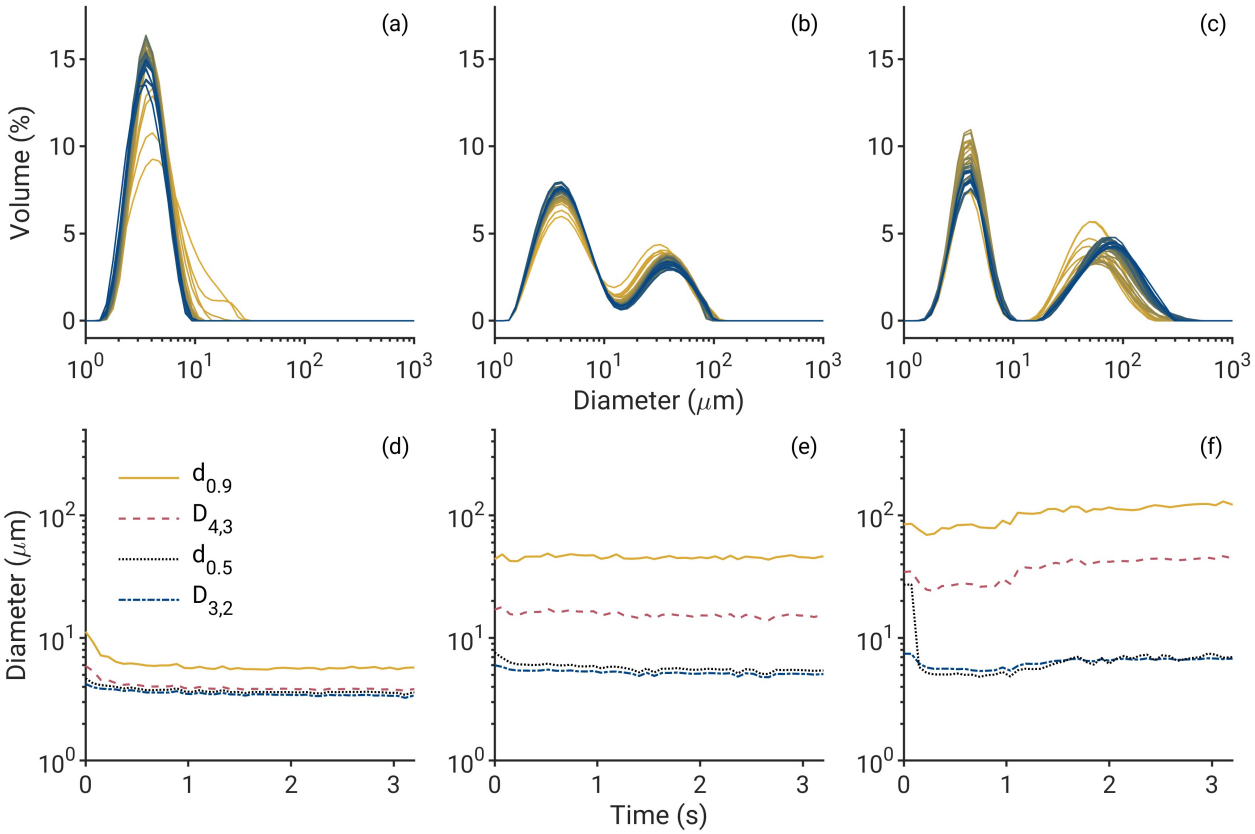

Fig. S4: (a–c) Volume distribution of *M. aeruginosa* suspensions at cell densities of 200, 400, and 800 μg/L Chl *a*. Each panel shows data from 43 measurements taken approximately every ≈74 s. Shades of yellow indicate earlier measurements, while blue represents later times. (d–f) Time evolution of $d_{0.9}$, $D_{4,3}$, $D_{3,2}$, and $d_{0.5}$. Stirring speed was 70 rpm during measurement.

Fig. S5 shows the obscuration data for *M. aeruginosa* suspensions at various cell concentrations. The obscuration levels ranged from approximately 3% to 20%, falling within the recommended range for the instrument used.[13]

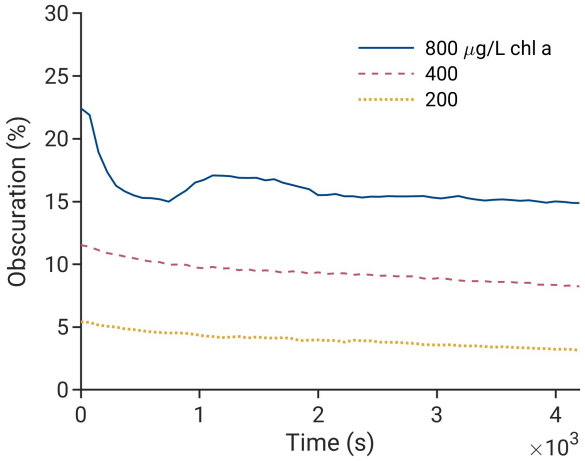

Fig. S5: Obscuration of *M. aeruginosa* cell suspensions at 800, 400, and 200 μg/L Chl a concentrations.

S4 Efficiencies of scattering using Mie theory

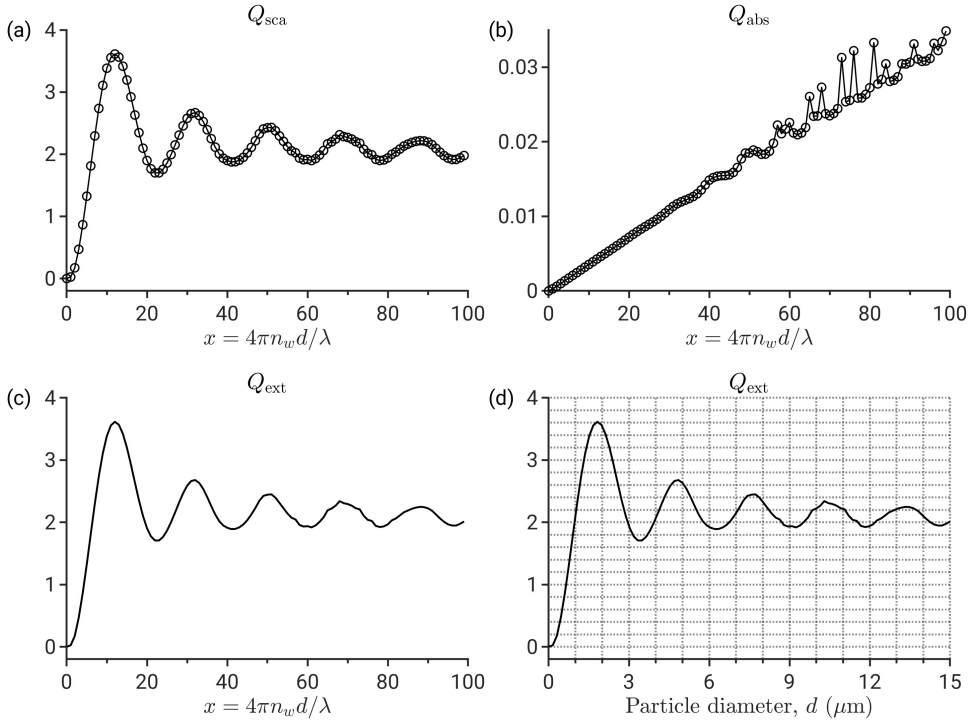

Fig. S6: Efficiencies of scattering (Q_{sca}), absorption (Q_{abs}), and extinction (Q_{ext}) versus particle size, calculated using Mie theory for particles with a refractive index of $m = 1.17 + 0.0001i$, where m is the complex refractive index of the algal cells relative to water.

Fig. S6 shows the efficiencies of scattering (Q_{sca}), absorption (Q_{abs}), and extinction (Q_{ext}) calculated using this value of particle refractive index. The variable, x, in Fig. S6(a–c) is

the product of the wavenumber, k, of light in the ambient medium (water) and the particle diameter, d.

$$k = \frac{4\pi}{\lambda_w} \tag{S2}$$

where λ_w is the wavelength in the water, given by the ratio of the light wavelength in the air ($\lambda = 633$ nm), and the refractive index of water ($n_w \approx 1.33$).

S5 Jar test procedure and results

Jar tests were conducted on 100 mL of *M. aeruginosa* cell suspensions in a 250 mL beaker, stirred magnetically at 60 rpm for 1 h. Alum was tested at concentrations ranging from 100 to 400 mg/L, while the *M. oleifera* extract was tested at concentrations ranging from 2 to 8 mL/L. After mixing, a 10-mL sample was transferred to a glass vial and allowed to settle for 1 h. Microscopic analysis using a Nikon Eclipse L200N optical microscope was performed on samples collected from the settled suspension. Representative results of the jar tests are shown in Fig. S7.

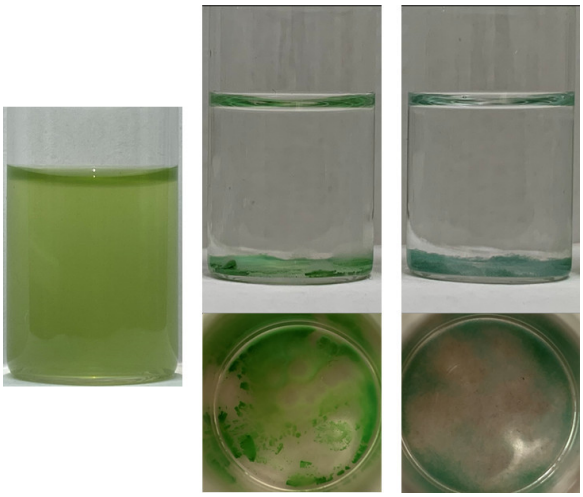

Fig. S7: Photographs of *Microcystis aeruginosa* cell suspension at 800 µg/L Chl *a*: (left) without flocculant, (center) with 2 mL/L DMSE, and (right) with 0.1 g/L alum suspension. Front and top views of flocculated suspensions.

S6 Floc size evolution of *M. aeruginosa* with alum

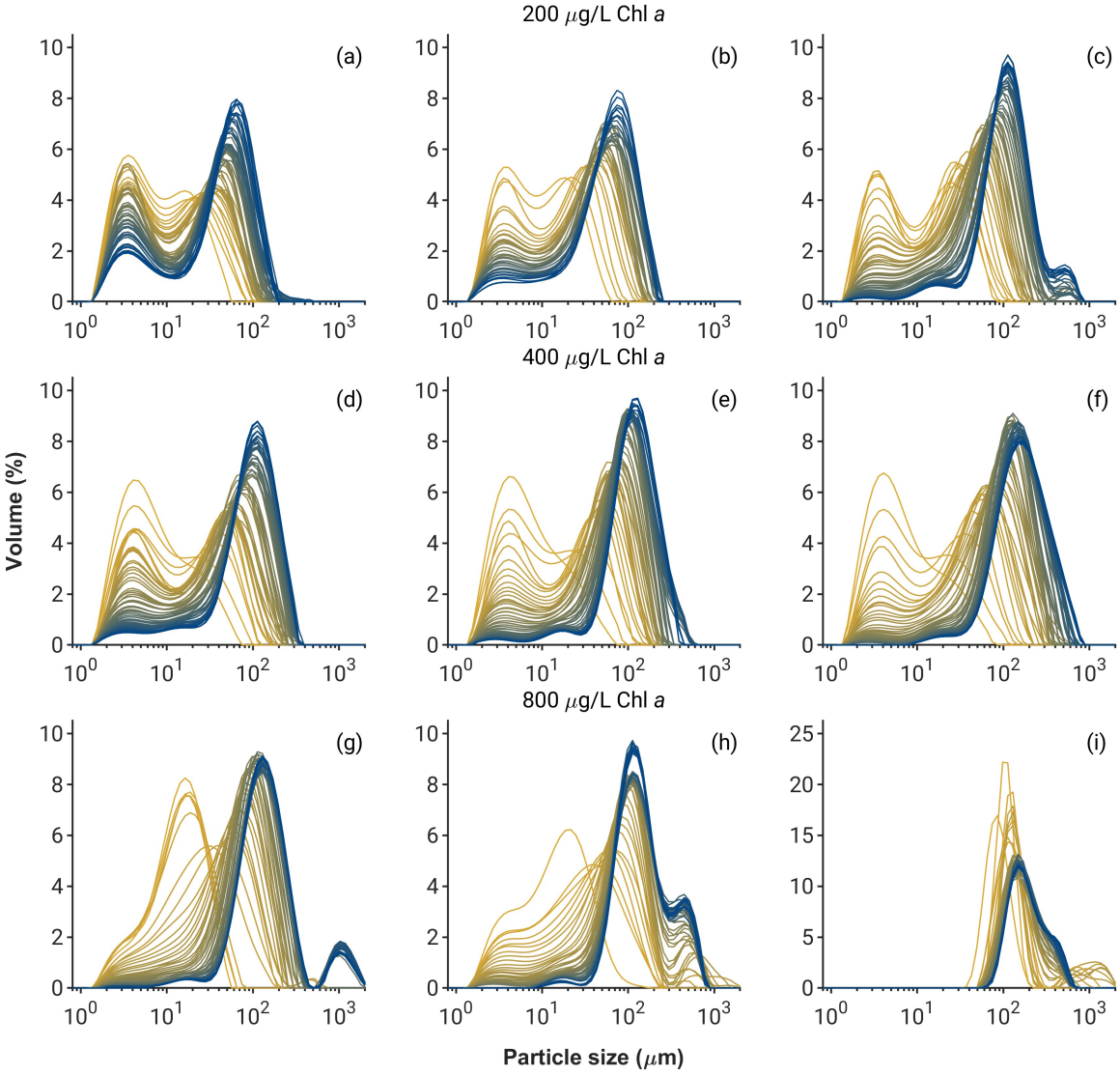

Fig. S8: Time evolution of the volume distribution of flocs in *M. aeruginosa* cell suspensions in the presence of alum. Top row: 200 μg/L Chl *a*. Middle row: 400 μg/L Chl *a*. Bottom row: 800 μg/L Chl *a*. Left column: 0.1 g/L alum. Center column: 0.2 g/L alum. Right column: 0.4 g/L alum. Size distribution measurement was made every ≈74 s. Stirring speed = 70 rpm.

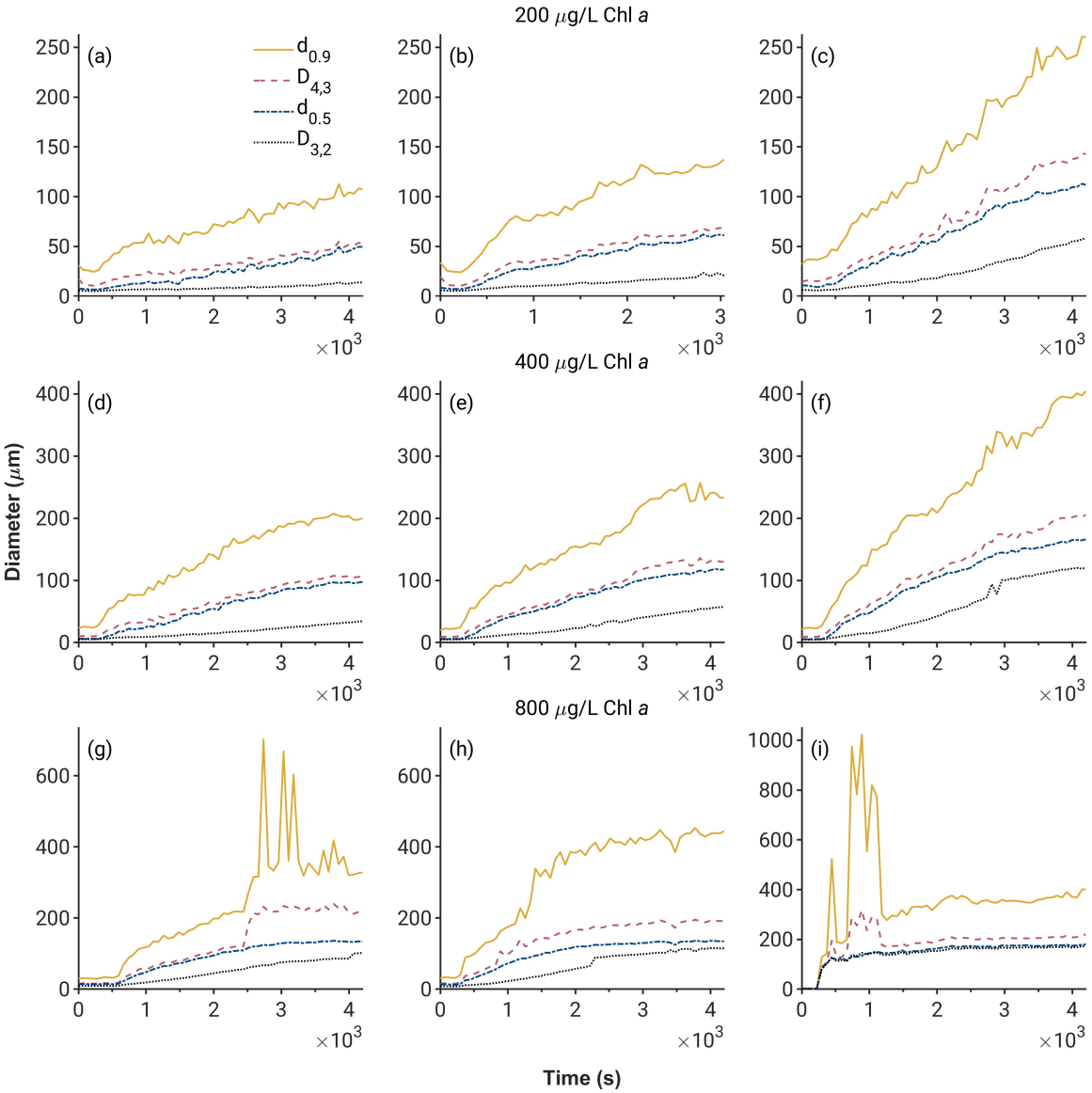

Fig. S9: Time evolution of floc diameters in *M. aeruginosa* cell suspensions in the presence of alum. Top row: 200 μg/L Chl *a*. Middle row: 400 μg/L Chl *a*. Bottom row: 800 μg/L Chl *a*. Left column: 0.1 g/L alum. Center column: 0.2 g/L alum. Right column: 0.4 g/L alum. Stirring speed = 70 rpm.

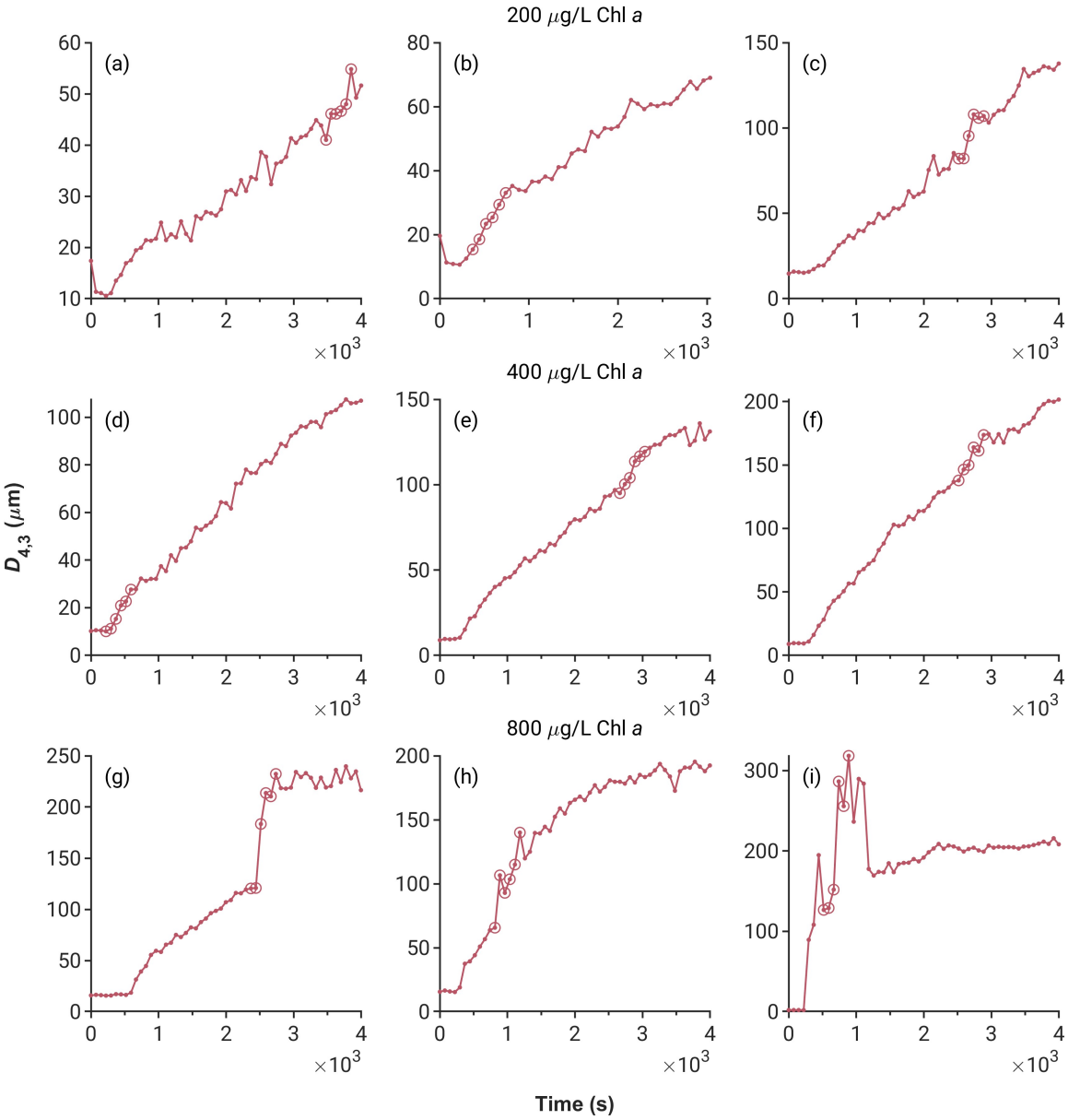

Fig. S10: Time evolution of $D_{4,3}$ of flocs in *M. aeruginosa* cell suspensions in the presence of alum. Top row: 200 μg/L Chl *a*. Middle row: 400 μg/L Chl *a*. Bottom row: 800 μg/L Chl *a*. Left column: 0.1 g/L alum. Center column: 0.2 g/L alum. Right column: 0.4 g/L alum. Circled points indicate the region of maximum local rate of rise in $D_{4,3}$.

S7 Floc size evolution of *M. aeruginosa* with *M. oleifera*

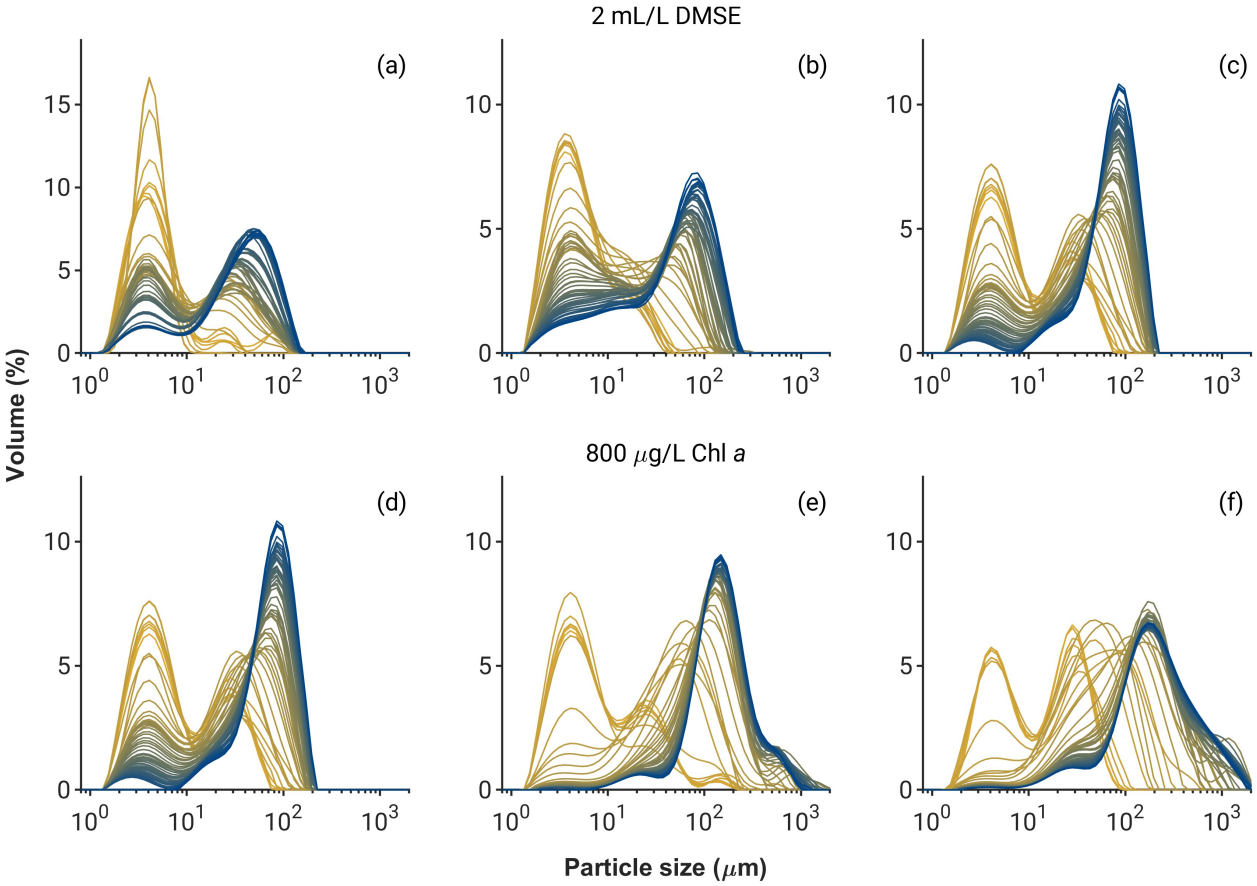

Fig. S11: Time evolution of floc volume distribution in *M. aeruginosa* cell suspensions. Top row: 2 mL/L DMSE with cell densities of 200, 400, and 800 μg/L Chl *a* (left to right). Bottom row: *M. aeruginosa* at 800 μg/L Chl *a*, with DMSE concentrations of 2, 6, and 8 mL/L (left to right). Measurements taken approximately every 74 s. Stirring speed = 70 rpm.

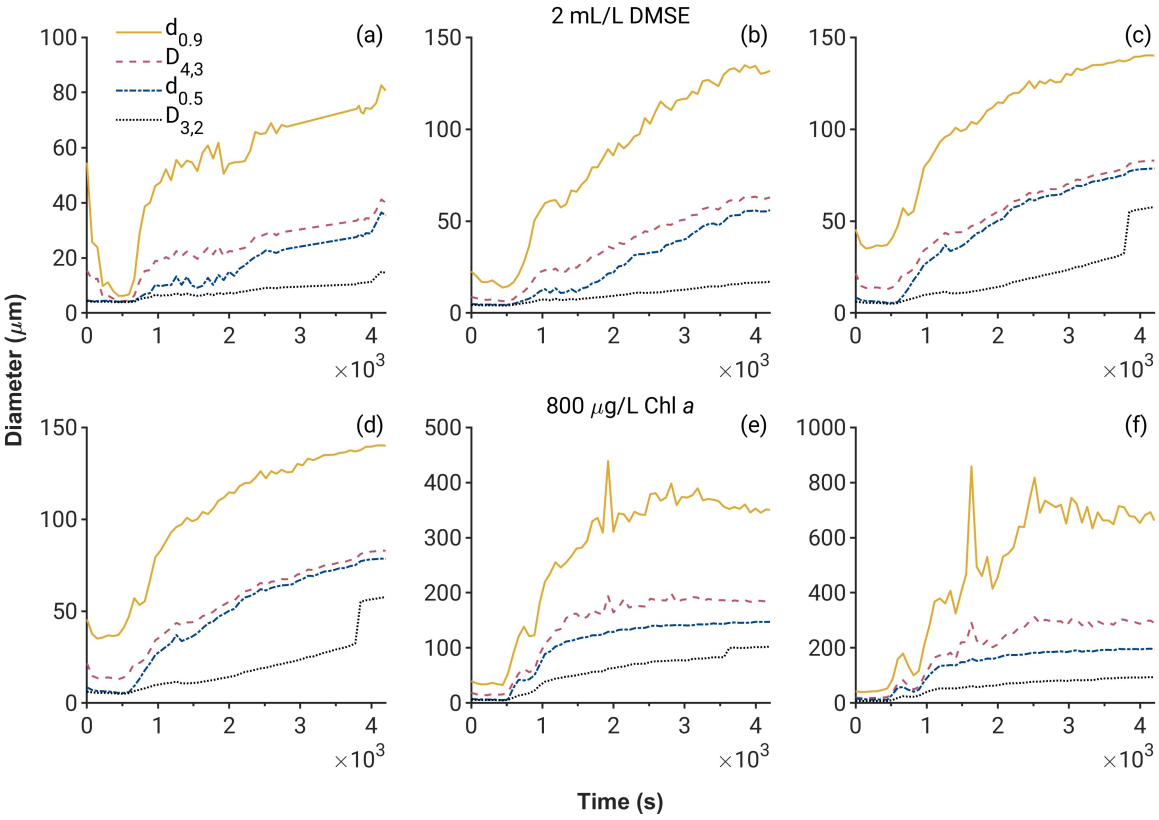

Fig. S12: Time evolution of floc diameters in *M. aeruginosa* cell suspensions. Top row: 2 mL/L DMSE with cell densities of 200, 400, and 800 μg/L Chl *a* (left to right). Bottom row: *M. aeruginosa* at 800 μg/L Chl *a*, with DMSE concentrations of 2, 6, and 8 mL/L (left to right). Measurements taken approximately every 74 s. Stirring speed = 70 rpm.

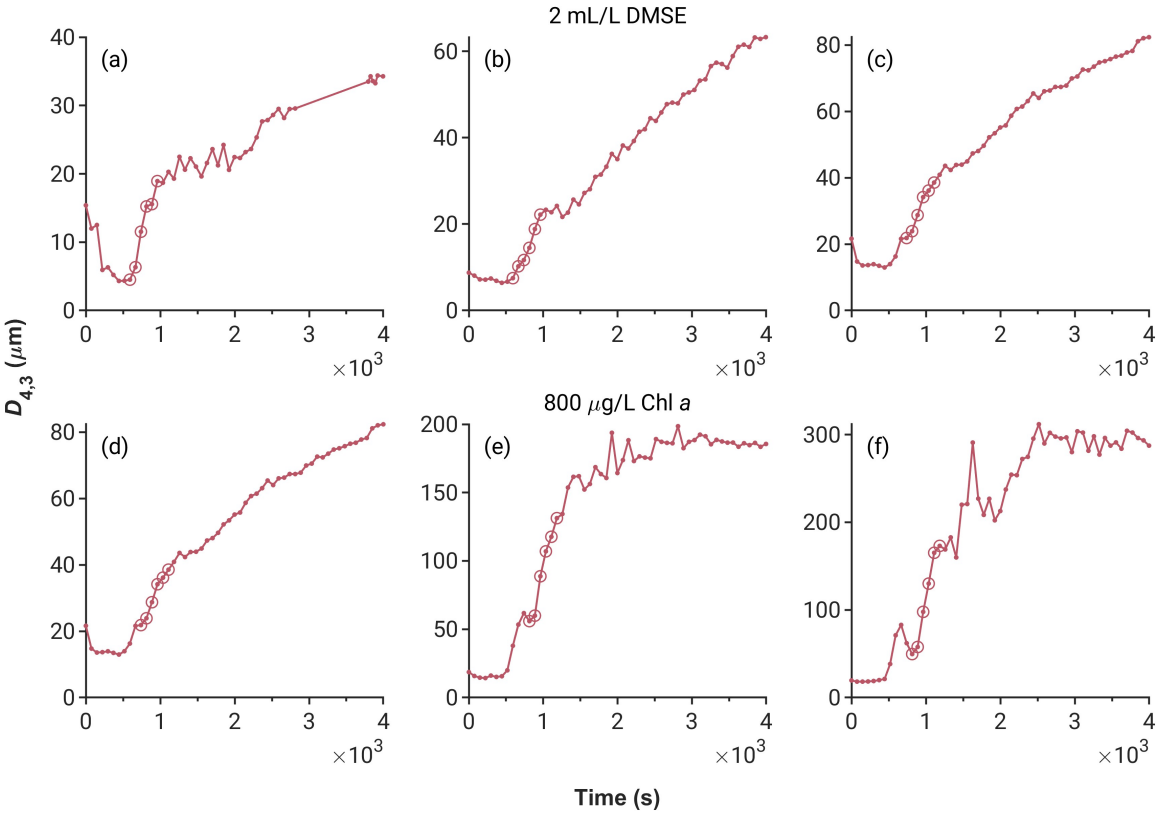

Fig. S13: Time evolution of $D_{4,3}$ of *M. aeruginosa* cell suspensions. Top row: 2 mL/L DMSE with cell densities of 200, 400, and 800 μg/L Chl *a* (left to right). Bottom row: *M. aeruginosa* at 800 μg/L Chl *a*, with DMSE concentrations of 2, 6, and 8 mL/L (left to right). Circled points indicate the region of maximum local rate of rise in $D_{4,3}$.

S8 Temporal profiles of fractal dimension

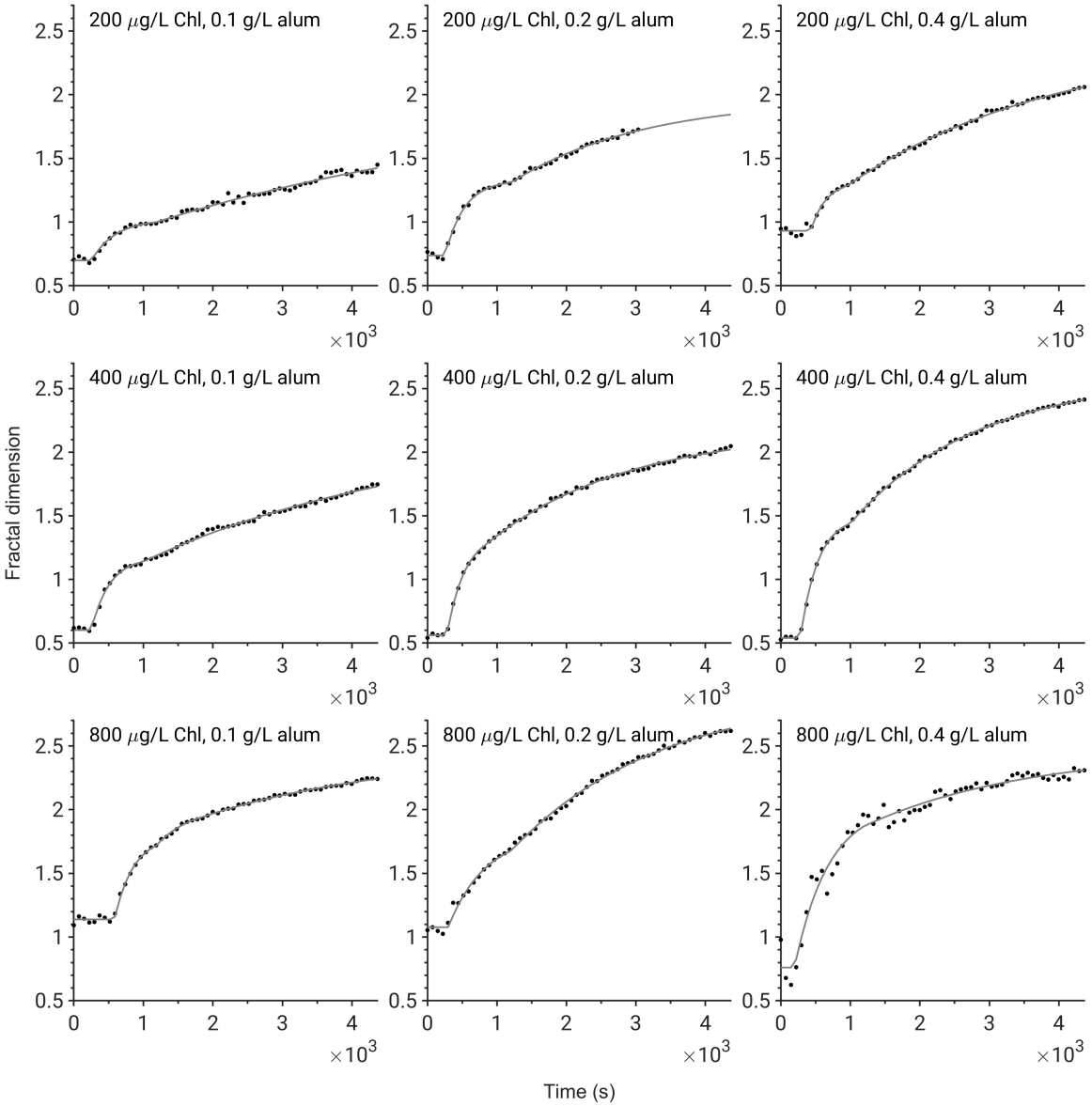

Fig. S14: Evolution of fractal dimension of *M. aeruginosa* flocs during alum-induced flocculation.

Fig. S14 shows the evolution of the fractal dimension in the flocculation of *M. aeruginosa* using alum. The symbols are experimental data, and the curves represent the fit of the data to the mathematical model in eqn (S3). This model is based on a first-order rate of increase [eqn (6) of the main article] and includes a delay time, t_0, to account for the induction period observed at the start of the measurements. In most experiments with alum, an initial rapid increase to a certain low fractal dimension, $d_{\mathrm{F},1}$, was followed by a slower restructuring to a higher value, $d_{\mathrm{F,max}}$. Therefore, the model incorporates two rate constants, k_1 and k_2,

corresponding to these two phases. Fig. S15 shows the fractal dimension evolution profiles for experiments using DMSE.

$$d_{\mathrm{F}} = \begin{cases} d_{\mathrm{F},0}, & \text{for } t \le t_0 \\ d_{\mathrm{F},1} - \left(d_{\mathrm{F},1} - d_{\mathrm{F},0}\right) \exp\left[-k_1 \left(t - t_0\right)\right], & \text{for } t_0 < t \le t_1 \\ d_{\mathrm{F,max}} - \left(d_{\mathrm{F,max}} - d_{\mathrm{F},1}\right) \exp\left[-k_2 \left(t - t_1\right)\right], & \text{for } t > t_1 \end{cases} \tag{S3}$$

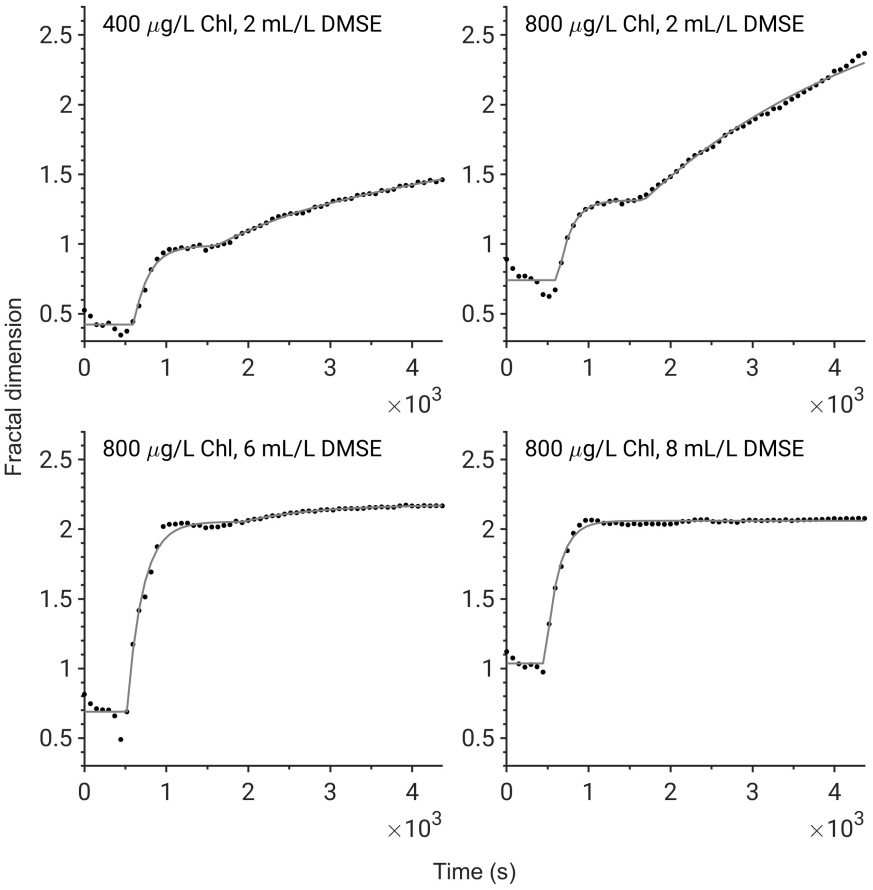

Fig. S15: Evolution of fractal dimension of *M. aeruginosa* flocs during flocculation induced by *M. oleifera*.

References

(1) U. Gassenschmidt, K. D. Jany, T. Bernhard and H. Niebergall, *Biochimica et Biophysica Acta*, 1995, **1243**, 477–481.

(2) J. E. C. Freire, I. M. Vasconcelos, F. B. M. B. Moreno, A. B. Batista, M. D. P. Lobo, M. L. Pereira, J. P. M. S. Lima, R. V. M. Almeida, A. J. S. Sousa, A. C. O. Monteiro-Moreira, J. T. A. Oliveira and T. B. Grangeiro, *PLOS ONE*, 2015, **10**, 1–24.

(3) A. Ndabigengesere and K. S. Narasiah, *Water Research*, 1998, **32**, 781–791.

(4) M. M. Özcan, *South African Journal of Botany*, 2020, **129**, 25–31.

(5) A. Ndabigengesere, K. S. Narasiah and B. G. Talbot, *Water Research*, 1995, **29**, 703–710.

(6) K. A. Ghebremichael, K. Gunaratna, H. Henriksson, H. Brumer and G. Dalhammar, *Water Research*, 2005, **39**, 2338–2344.

(7) A. Jain, R. Subramanian, B. Manohar and C. Radha, *Journal of Food Science and Technology*, 2019, **56**, 2093–2104.

(8) N. A. Oladoja and G. Pan, *Sustainable Chemistry and Pharmacy*, 2015, **2**, 37–43.

(9) F. P. Camacho, V. S. Sousa, R. Bergamasco and M. Ribau Teixeira, *Chemical Engineering Journal*, 2017, **313**, 226–237.

(10) G. S. Madrona, G. B. Serpelloni, A. M. Salcedo Vieira, L. Nishi, K. C. Cardoso and R. Bergamasco, *Water, Air, & Soil Pollution*, 2010, **211**, 409–415.

(11) T. Okuda, A. U. Baes, W. Nishijima and M. Okada, *Water Research*, 1999, **33**, 3373–3378.

(12) Pierce Biotechnoloy, *Pierce Biotechnology Technical Resource, TR0006.0: Extinction Coefficients*, 2002.

(13) *Mastersizer 2000 User Manual, Malvern Instruments*, 2007.